PALEONTOLOGY

Late acquisition of erect hindlimb posture and function in the forerunners of therian mammals

Peter J. Bishop[1,2]* and Stephanie E. Pierce[1]

The evolutionary transition from early synapsids to therian mammals involved profound reorganization in locomotor anatomy and function, centered around a shift from "sprawled" to "erect" limb postures. When and how this functional shift was accomplished has remained difficult to decipher from the fossil record alone. Through biomechanical modeling of hindlimb force-generating performance in eight exemplar fossil synapsids, we demonstrate that the erect locomotor regime typifying modern therians did not evolve until just before crown Theria. Modeling also identifies a transient phase of increased performance in therapsids and early cynodonts, before crown mammals. Further, quantifying the global actions of major hip muscle groups indicates a protracted juxtaposition of functional redeployment and conservatism, highlighting the intricate interplay between anatomical reorganization and function across postural transitions. We infer a complex history of synapsid locomotor evolution and suggest that major evolutionary transitions between contrasting locomotor behaviors may follow highly nonlinear trajectories.

INTRODUCTION

A key objective in the study of macroevolution is deciphering the patterns and processes by which new clades and body plans arise. Of particular interest are instances involving great transformations in organismal biology (*1*, *2*), where evolving lineages transition between radically different suites of anatomy, function, physiology, behavior, and ecology. The reorganization of the synapsid locomotor system is one such example, as it formed a cornerstone to the ecological radiation of mammals in the Cenozoic (*3*, *4*). Central to this was a shift from reptile-like "sprawled" postures, with the limbs held to the side of the body, to the "erect" postures of therians (marsupials and placentals), with the limbs held close to the body midline. In addition to kinematic differences, sprawling and erect locomotion involve marked differences in stability, musculoskeletal mechanics, neural control, and bone loading (*5*–*9*). Understanding how synapsids transitioned between these two contrasting modes of locomotion can therefore illuminate the ways in which major, clade-defining phenotypic changes can evolve.

The transformation of locomotor anatomy in the nonmammalian synapsid ancestors of mammals is documented by an exceptional fossil record spanning 100+ million years (Ma) (*10*–*15*), but interpreting this record has proved challenging. Through disparate lines of evidence and reasoning, prior studies frequently conflict in their assessment of locomotor posture in noncynodont therapsids (hereafter "therapsids"), nonmammalian cynodonts (hereafter "cynodonts"), stem monotremes, and stem therians [e.g., (*10*, *16*, *17*–*25*)]. There is consequently little consensus on when the erect locomotor behavior of extant therians first evolved. By current estimates, some taxa apparently used sprawled forelimb postures but more erect hindlimb postures (*10*, *16*, *17*, *21*, *22*, *24*, *26*, *27*–*29*), a paradoxical configuration not observed among extant tetrapods. Moreover, anatomical and functional shifts in individual body systems often do not appear to phylogenetically coincide with those occurring in other systems (*10*–*15*, *22*, *30*–*35*), complicating interpretations of the sequence or mechanism of functional transformation. Arguing against a simple, gradualistic (linear) narrative of locomotor evolution, Kemp (*10*, *16*, *23*, *36*) proposed that advanced therapsids and early cynodonts were facultatively capable of a broad range of limb postures, akin to extant crocodylians (*37*, *38*), before a committed shift to exclusively erect postures in advanced cynodonts. This hypothesis implies that a transient phase of increased locomotor versatility (*39*) was a key facilitator of the evolution of novel locomotor behaviors on the line to mammals (*40*).

Clarifying the functional meaning of fossil anatomies and their transformation across deep time necessarily requires recourse to data from extant species. However, phenomenological perspectives alone may have limited predictive value for the entire 320+-Ma history of Synapsida. By contrast, approaches grounded in universal physical and biological principles can mechanistically relate form, function, and behavior in a robust and quantitative fashion across deep time (*39*–*42*). Increasingly, this has involved the development of computational biomechanical models of the locomotor system (*41*, *43*), which typically focus on the function of individual muscles or joints [e.g., (*17*, *44*, *45*–*50*)]. Although informative, these studies seldom address the interactions between different musculoskeletal units, such as muscle multiarticularity, agonist-antagonist cocontraction, and redundancy in the musculoskeletal system, where there are more muscles than degrees of freedom (DOF) (*39*, *41*, *51*). These complexities of muscle-joint codependence throughout a limb are best captured through linear algebra (*39*, *51*) and remain unaccounted for by simpler, arithmetic summation of muscle moment arms or moments for a given joint [e.g., (*34*, *44*, *47*, *50*)], obfuscating the relationships between anatomy, mechanics, and whole-animal behavior [e.g., (*52*, *53*)].

Here, we take a more holistic approach to synapsid locomotor evolution by modeling functional performance at the level of the whole limb, in addition to the action of individual muscle units. We apply the concept of a feasible force space (FFS) (*39*, *54*) to the fossil record and quantify the maximum force that a limb can apply on the external environment in all directions, a key determinant of whole-animal performance in locomotion (*55*–*57*). In circumscribing a limb's three-dimensional force-producing capacity at a global level, FFSs implicitly capture all potential interactions among different muscles and joints throughout the limb (*39*, *54*). Their study can

[1]Museum of Comparative Zoology and Department of Organismic and Evolutionary Biology, Harvard University, Cambridge, MA, USA. [2]Geosciences Program, Queensland Museum, Brisbane, Queensland, Australia.
*Corresponding author. Email: pbishop@fas.harvard.edu

therefore provide a unique perspective for interpreting musculoskeletal anatomy and function and offer a broader view of "locomotor regime" than joint posture alone, facilitating a more nuanced assessment of synapsid locomotor evolution. Given that postural transformation on the line to mammals occurred within the context of terrestrial locomotion (*10*, *22*, *40*), we here focus on the hindlimb, the main source of propulsion in terrestrial locomotion, simultaneously avoiding complexities associated with potential ecological specialization of the forelimb for other behaviors. To achieve this, we draw upon recent work on synapsid appendicular evolution (*14*) and the scaling of appendicular musculature in extant amniotes (*58*) to estimate missing soft tissues and their properties in extinct taxa (*59*).

To quantitatively link anatomy, function, and whole-limb performance across the sprawling-to-erect transition in synapsids, we study five extant and eight extinct taxa that phylogenetically and functionally bracket this transition (Fig. 1A and Table 1). The extant taxa collectively span the postural continuum from sprawled to erect, whereas the extinct taxa are well-known exemplars of their respective clades, collectively representing each "grade" of synapsid evolution and capturing the major hindlimb musculoskeletal changes that occurred on the line to therians (*14*, *59*). We develop a user-friendly pipeline for rapid computation of FFSs and muscle actions, which can be deployed to diverse musculoskeletal systems, and test the plausibility of Kemp's (*16*) "postural flexibility" hypothesis. We find that while advanced therapsids and early cynodonts likely had greater locomotor versatility compared to their ancestors, this was followed by a sustained reversal in locomotor performance in later diverging synapsids—casting doubt on the importance of increased versatility in facilitating major evolutionary shifts in locomotor mechanics. Furthermore, our results indicate a late acquisition of therian-like hindlimb function, well within stem therians. Quantification of major hip muscle actions identifies divergent patterns of functional change and conservatism, underscoring the intricate interplay between anatomical reorganization, posture, and function throughout synapsid evolution. By exploring synapsid hindlimb function from both whole-limb and muscle-centric perspectives, our results highlight a (previously unrecognized) complex and protracted nature to the sprawling-to-erect transition.

RESULTS

Hindlimb performance and posture

For each taxon, we quantified hindlimb performance by computing a three-dimensional FFS (Fig. 1B), an envelope that delineates the range of forces that can be applied by the limb on the external environment, in terms of both magnitude and direction (*39*, *54*). Points on the envelope's surface denote maximal performance, corresponding to a single unique combination of muscle recruitment, whereas points within the envelope's interior are achievable by multiple different muscle recruitment patterns. The FFSs were calculated via an optimization-based approach across a wide range of postures spanning a continuum of whole-limb adduction (i.e., how sprawled or erect the limb is), flexion, and forward-backward pitch (Fig. 1, C and D, and see Materials and Methods). These postures define what is "kinematically feasible" for a particular model, given the constraints of segment proportions, joint axis orientations, and foot placement (Fig. 1C), but because of ostensible joint disarticulation or bone collision, not all of these poses will necessarily be "osteologically viable" and, hence, attainable in life. For each posture tested, we extracted force-producing capacity in each "cardinal direction," the cube root of FFS volume (CRV; i.e., overall capacity), and how FFS volume partitions into different directions (Fig. 1B). As our study taxa vary greatly in body size (Table 1), all performance metrics were normalized by the average maximum strength of the muscles in a given model, expressing performance in "muscle strength units" (MSUs; see Materials and Methods). This describes how efficiently internal muscular force is converted to external environmental force, irrespective of body size.

Size-normalized force-producing capacity varies markedly with the degree of hindlimb adduction, and the manifestation of this variation differs substantially across taxa (Figs. 2 and 3 and fig. S1). To contextualize this variation, it is notable that in all extant taxa, CRV is at or near its maximal value at adduction angles corresponding to the posture(s) each habitually uses (Fig. 2B, black lines and yellow vertical bars), as recorded by in vivo studies of steady-state locomotion (*38*, *60*–*65*). This correlation suggests that CRV can provide insight into posture in extinct species, and it is sensible that CRV should correlate with habitual posture. In the stance phase of locomotion, being able to exert large substrate forces in a wide range of directions affords the limb greater functional flexibility, especially in unsteady behaviors such as acceleration or turning (*57*, *66*). Similarly, in the swing phase, it would be beneficial to be able to generate meaningful accelerations of the foot and, thus, reposition it sufficiently quickly in many directions. The magnitude of force in the ventral direction (F_V), a direct measure of weight-bearing capacity, also shows a notable correlation with habitual posture (Fig. 2A, red lines). In four of the five extant taxa, F_V is maximal around the habitual posture(s) used, but in *Salvator*, it is the highest in a more erect posture than that which is habitually used (Fig. 2A). Across all extant and extinct taxa, lateral force capacity (F_L) is ubiquitously higher in more sprawled poses (Figs. 2 and (3, purple lines), which would enhance turning or agility in those poses (*55*, *67*). We find little evidence for a correlation between any other performance metric and posture.

Within the extinct species (Fig. 3), the "pelycosaurs" (nontherapsid synapsids) *Ophiacodon* and *Dimetrodon* are notably limited in the adduction angles they can achieve in osteologically viable postures, at both ends of the postural continuum, paralleling observations of the forelimb (*15*, *46*, *68*). The advanced cynodont *Megazostrodon* and the stem-therian *Vincelestes* are also osteologically incapable of assuming strongly adducted (i.e., more erect) poses. Although variation in force-producing capacity across the taxa is considerable, the pelycosaurs exhibit their own distinct patterns, as do the therapsids (*Oudenodon*, *Lycaenops*, and *Regisaurus*) and the cynodont *Massetognathus*, especially in terms of FFS volume partitioning (Fig. 3B). These are suggestive of marked differences in hindlimb locomotor styles between the sampled pelycosaurs and more derived synapsids. Apart from *Vincelestes*, total CRV is maximized around adduction angles of 30° to 40°, similar to the results obtained for the extant *Didelphis* and *Tachyglossus* (Figs. 2B and 3B, black lines). However, in other metrics of force-producing capacity, there is far less consistency, and all extinct species' patterns deviate (qualitatively and quantitatively) from those observed in the extant species in their own, unique ways.

To avoid reliance on singular metrics for characterizing locomotor function, we also define each taxon's hyperdimensional "performance profile" as the collective aggregation of all performance metrics across all combinations of adduction, flexion, and pitch (osteologically viable postures only). To characterize how "therian-like" each taxon's performance profile is, we calculated the Pearson correlation between

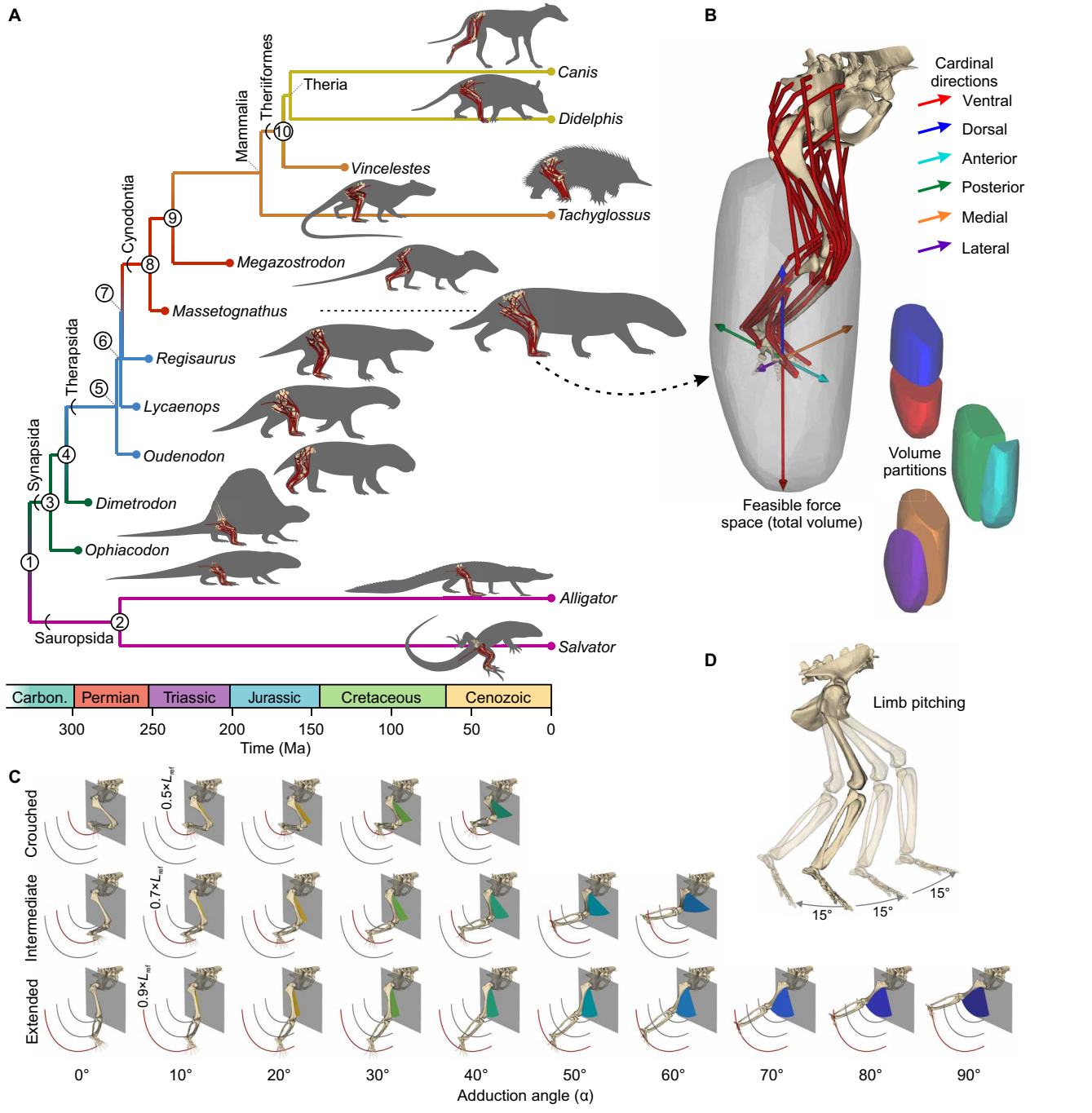

Fig. 1. Summary of approach to investigating hindlimb force-producing ability. (**A**) Time-calibrated phylogeny of study taxa, showing musculoskeletal models of the hindlimb; silhouettes not to scale. Numbered nodes are as follows: 1, Amniota; 2, Sauria; 3, Metopophora; 4, Sphenacodontoidea; 5, Neotherapsida; 6, Theriodontia; 7, Eutheriodontia; 8, Eucynodontia; 9, Mammaliaformes; 10, Prototribosphenida. (**B**) Example FFS for the cynodont *Massetognathus*, showing total volume and force magnitudes in each cardinal direction. (**C**) Force spaces were computed across a range of limb postures, with the base set of postures spanning a continuum of adduction (sprawled to erect) and flexion (crouched to extended, based on limb reference length L_{ref}; see Materials and Methods), shown here with *Massetognathus*. Note that while 30 combinations of adduction and flexion potentially exist, certain ones will not be kinematically feasible for various taxa because of the constraints of limb segment proportions and joint axis orientations. (**D**) The base set of postures was pitched forward and back at the hip to generate the full suite of postures explored.

Table 1. Taxa and focal specimens used in the study. AMNH, American Museum of Natural History, New York, NY, USA; BP, Evolutionary Studies Institute, University of the Witwatersrand, Johannesburg, South Africa; FMNH, Field Museum of Natural History, Chicago, IL, USA; MACN, Museo Argentino de Ciencias Naturales "Bernardino Rivadavia," Buenos Aires, Argentina; MCZ, Museum of Comparative Zoology, Harvard University, Cambridge, MA, USA; NHMUK, Natural History Museum, London, UK; SEP, Pierce Lab research collection.

Taxon	Clade	Age	Focal specimen	Hindlimb completeness	Body mass (kg)*
Salvator merianae	Squamata	Recent	SEP73	100%	1.04
Alligator mississippiensis	Crocodylia	Recent	#3 (*38*)	100%	3.6
Ophiacodon retroversus	Ophiacodontidae	Early Permian, 296.4 Ma	FMNH UC 458	Near-complete, femoral epiphyses poorly ossified	88.489
Dimetrodon milleri	Sphenacodontidae	Early Permian, 290.1 Ma	MCZ VPRA-1365	Complete, femur taphonomically distorted	32.599
Oudenodon bainii	Dicynodontia	Late Permian, 259.9 Ma	NHMUK PV R.4067	Near-complete pelvis, femur, tibia, and fibula	51.609
Lycaenops ornatus	Gorgonopsia	Late Permian, 259.9 Ma	AMNH FARB 2240	Near-complete pelvis, femur, tibia, and fibula; pes minimally accessible	40.15
Regisaurus jacobi	Therocephalia	Early Triassic, 252.2 Ma	BP/1/5394	Complete ilium, femur, tibia, fibula, astragalus, and calcaneum	3.6
Massetognathus pascuali	Cynognathia	Middle Triassic, 242 Ma	MCZ VPRA-3691	Complete ilium, partial pubis, and complete femur and tibia	1.137
Megazostrodon rudnerae	Morganucodontidae	Early Jurassic, 201.3 Ma	NHMUK PV M.26407	Complete ilium, ischium, and femur, partial tibia and fibula, and near-complete pes	0.0354
Tachyglossus aculeatus	Monotremata	Recent	SEP42	100%	3.31
Vincelestes neuquenianus	Cladotheria	Early Cretaceous, 129.4 Ma	MACN-N 09/39	Near-complete pelvis, femur, tibia, fibula, astragalus, and calcaneum	0.983
Didelphis virginiana	Marsupialia	Recent	SEP87	100%	2
Canis familiaris	Placentalia	Recent	(*92*)	100%	23.9

*Estimated for extinct taxa using minimum humerus and femur circumferences (*98*).

its profile and the profile for *Canis* (see Materials and Methods). This illustrates a clear decoupling between the optimal adduction angle that maximizes CRV and how therian-like a given taxon is (Fig. 4A), highlighting the pitfalls of overreliance on any one metric (*37*). The locomotor regime of the extant therians is characteristic of just these two taxa; as illustrated in Fig. 2, this may be typified by high CRV and F_V in erect postures, a tendency for greater posterior force-producing capacity in more erect postures, and an inability to assume strongly sprawled (yet osteologically viable) postures. Ancestral state reconstruction illustrates a complex evolutionary trajectory on the line to therians (Fig. 4A), with a reversal toward less therian hindlimb function around Eucynodontia, and a shift back toward more therian function at crown Theria. Agglomerative hierarchical cluster analysis of performance profiles provides additional insight into variation across taxa (Fig. 4B and see Materials and Methods). If the transition from sprawling to erect locomotor regimes was linear, a "Hennigian comb"–like cluster profile would be expected. Instead, we recovered a starkly different pattern defined by two major types of performance profile: both pelycosaurs and all nontherian mammaliaforms cluster with *Salvator* in a "sprawling" group to the exclusion of other taxa ("nonsprawling"). Notably, the performance profiles of the therapsids and, especially, the cynodont *Massetognathus* are most similar to that of *Alligator*, which uses a range of limb postures during locomotion (*37*, *38*).

Performance through time

We used ancestral state reconstruction to explore how hindlimb force-producing performance evolved in Synapsida. As some of the postures we sampled are unlikely to have been used in vivo by a given taxon, we focused on the adduction angle that maximized CRV (averaged across levels of limb flexion and pitch; Figs. 2 and (3), to provide a "snapshot" of the posture most likely to be used in each taxon. At this adduction angle, we computed the mean performance value across all combinations of flexion and pitch for each metric and repeated the process for each taxon; we then used these means to estimate the evolution of hindlimb performance along the stem lineage (see Materials and Methods). Every metric exhibits a significant trend along the mammalian stem lineage (Fig. 5 and fig. S2). Posterior force-producing capacity increases more or less monotonically (Fig. 5A, green line), indicating improved ability for forward

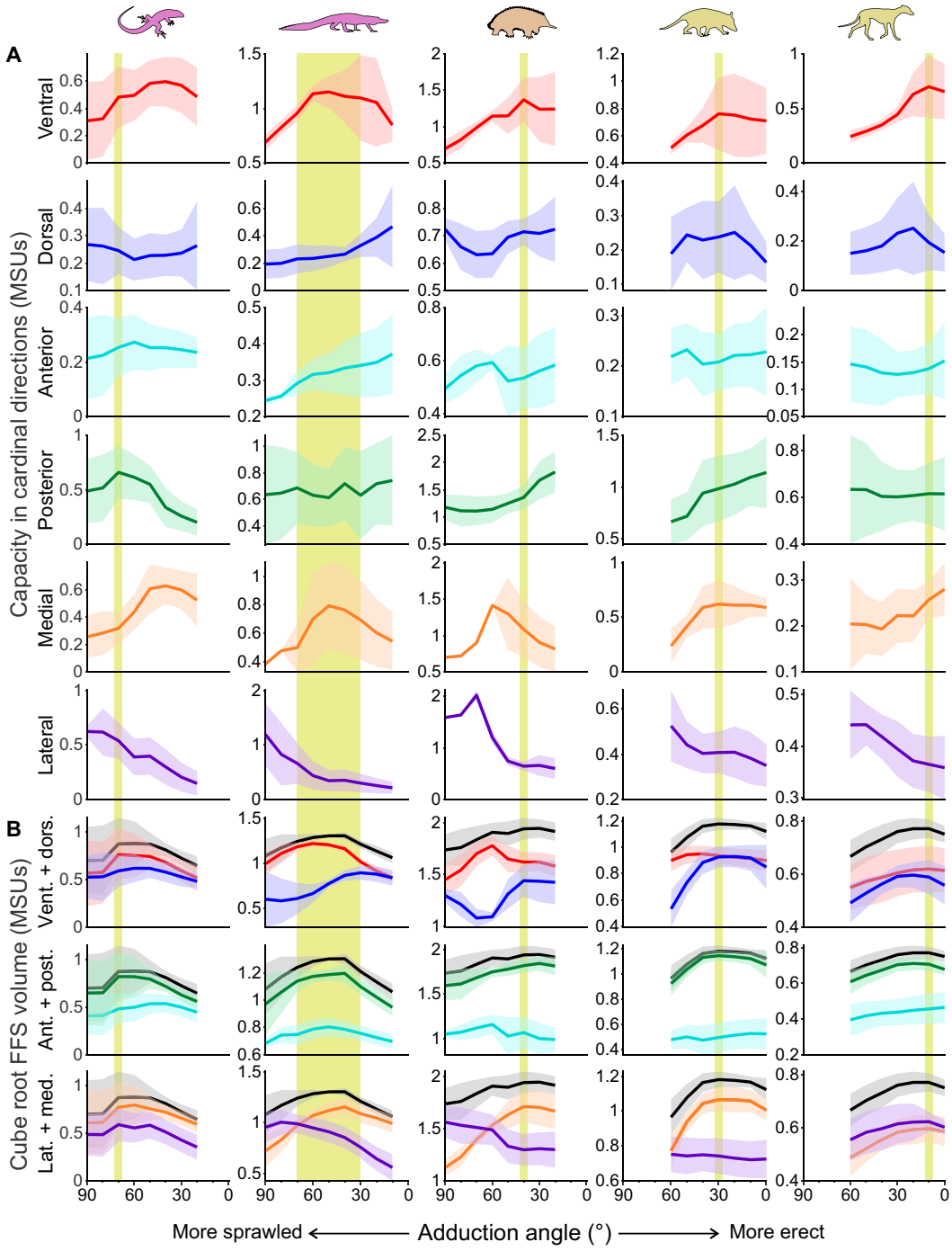

Fig. 2. Covariation of performance and hindlimb posture in extant taxa. (**A**) Force-producing capacity in the cardinal directions. (**B**) CRV (black line and gray shading) and cube root of each of the ventral, dorsal, anterior, posterior, lateral, and medial partitions of FFS volume (see Fig. 1B for color codes). Results reported as means ± SD (expressed in MSUs) across osteologically viable postures only, across all levels of whole-limb flexion and pitch. An adduction angle of 0° denotes fully erect, whereas 90° denotes fully sprawled. Yellow vertical bars signify habitually used postures, as determined from in vivo locomotor data (see Materials and Methods for data sources). From left to right, taxa are *Salvator*, *Alligator*, *Tachyglossus*, *Didelphis*, and *Canis*. See fig. S1 for results for all kinematically feasible postures.

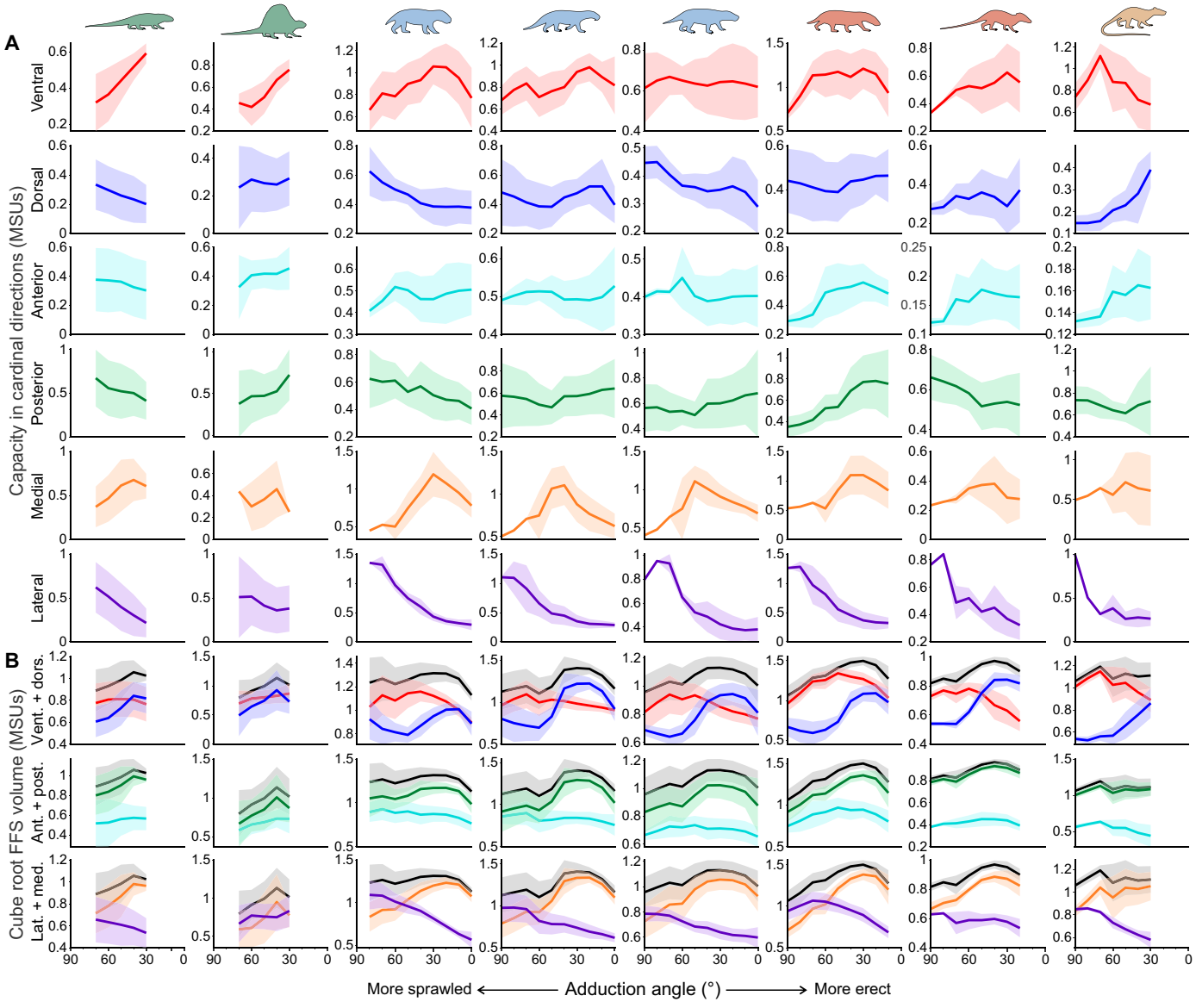

Fig. 3. Covariation of performance and hindlimb posture in extinct synapsids. (**A**) Force-producing capacity in the cardinal directions. (**B**) CRV and cube root of each of the ventral, dorsal, anterior, posterior, lateral, and medial partitions of FFS volume. From left to right, taxa are *Ophiacodon*, *Dimetrodon*, *Oudenodon*, *Lycaenops*, *Regisaurus*, *Massetognathus*, *Megazostrodon*, and *Vincelestes*. Conventions as per Fig. 2; only results for osteologically viable postures are shown. See fig. S1 for results for all kinematically feasible postures.

acceleration on the line to Theria. This correlates with an increasing proportion of total FFS volume being partitioned in the posterior direction along the stem lineage (Figs. 2B and 3B). Many other metrics increase and then decrease along the stem lineage: Performance increases in therapsids, reaching an acme around Eucynodontia, before decreasing within mammals. Thus, once corrected for size, therapsids and early cynodonts were especially effective at converting muscular forces into external forces applied on the environment in diverse directions.

Hip muscle function

Complementing our assessment of whole-limb performance, we explored the functional consequences of reorganization in hindlimb musculature during synapsid evolution (*14*, *59*). We focus on four hip muscle groups that underwent major transformation on the line to mammals: iliofemoralis (IF) → gluteals (GLUT), anterior iliotibialis (ITa) → rectus femoris (RF), ambiens (AMB) → sartorius (SART), and puboischiofemoralis internus (PIFI) → iliopsoas (ILPS). For each muscle, we computed their "kinematic potentials" (KPs; Fig. 6A) across the range of postures tested for each taxon. KPs describe the ability of individual muscles to move the whole limb in a particular direction in a given posture, expressed as foot motion in the global reference frame (see Materials and Methods).

The IF group runs from the ilium dorsal to the acetabulum to the lateral proximal femur. On the line to mammals, the muscle differentiates, its iliac origin expands anteriorly, and its femoral

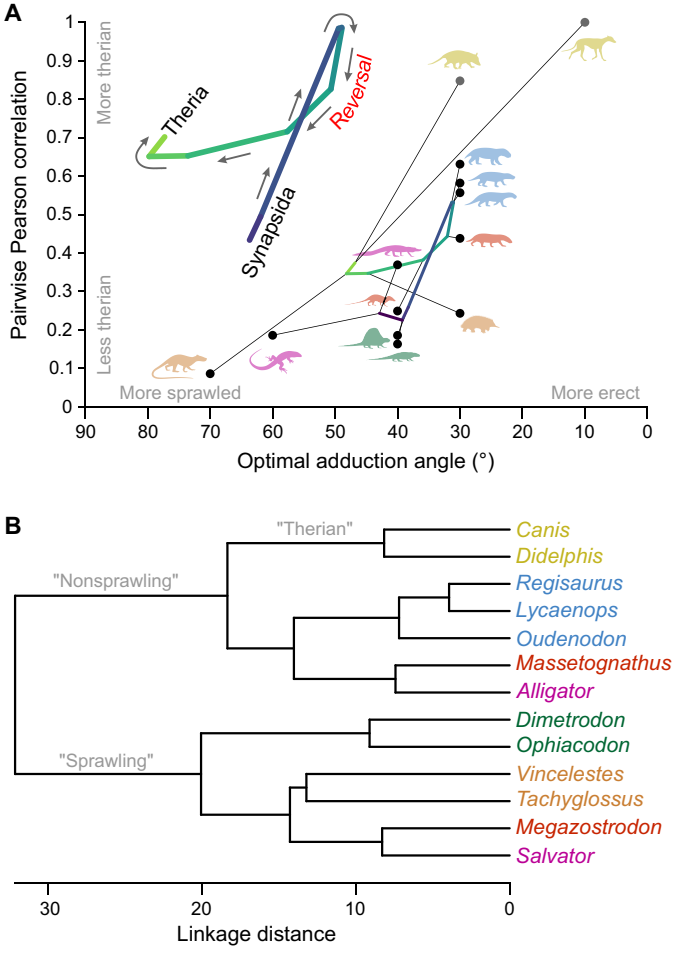

Fig. 4. Hindlimb hyperdimensional performance profiles across extant and extinct taxa. (**A**) Phyloplot of optimal adduction angle (angle at which total CRV is maximal) and Pearson's correlation for pairwise comparisons of performance profiles between each taxon and *Canis*. Thick colored line denotes ancestral state reconstruction of locomotor regime along the stem lineage; note the reversal in evolutionary trend, toward less therian-like performance profiles, initiated in early cynodonts. (**B**) Dendrogram of hierarchical similarity of each taxon's performance profile, showing two major types of performance profile, sprawling and nonsprawling.

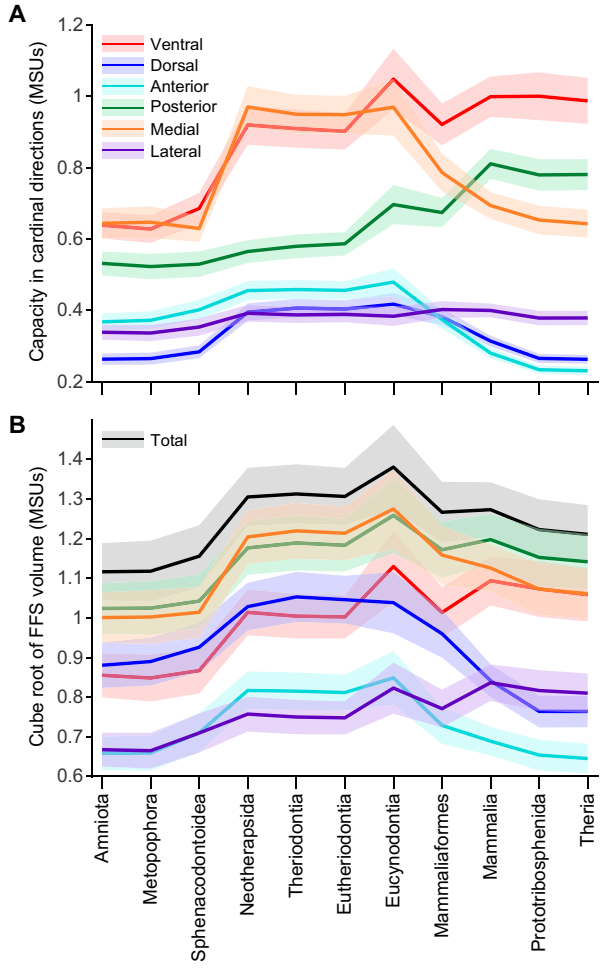

Fig. 5. Ancestral state reconstruction of hindlimb performance in Synapsida. (**A**) Maximum force-producing capacity in the cardinal directions, reported in MSUs, whereby force is normalized to mean muscle F_{max}. (**B**) CRV, as a whole and partitioned into each direction. Results are of means ± SD of output from Monte Carlo simulations with random perturbations of up to ±20%; the same fundamental patterns are recovered even when input performance data are perturbed by up to ±50%. See also fig. S2.

insertion develops into the greater trochanter, producing the GLUT. Despite this transformation, KPs vary with adduction angle in a broadly similar fashion across all taxa (Fig. 6B): More sprawled poses lead to a greater tendency for dorsal foot motion, but more erect poses lead to a greater tendency for lateral foot motion. This reflects a consistent capacity for hip elevation (and internal rotation) across postures (fig. S3A) and is consilient with the presumed functional shift of this muscle group in synapsid evolution (*25*): from a limb elevator in sprawled poses (recruited in swing phase) (*69*, *70*) to a limb abductor for mediolateral stability in erect poses (recruited in stance phase) [e.g., (*71*)]. Superimposed on this conserved pattern, the area of the unit sphere that is accessible by KPs also increases over time, most notably from pelycosaurs to therapsids (fig. S4, A and B), coinciding with anterior iliac expansion and initial development of the greater trochanter, as well as the ability to assume a wider range of limb adduction in therapsids onward (Fig. 3). This would have enabled greater directional versatility in how the IF could contribute to hindlimb motion during swing or stance. KPs also acquire a greater anterior component in *Dimetrodon*, which progressively increases through therapsids, cynodonts, and mammals (Fig. 6B), driven by the anterior expansion of the muscle's iliac origin. As the IF originates more anteriorly to the hip, its subdivisions progressively lose the capacity for hip retraction and become more effective at protraction (fig. S3A); acquisition of protraction capacity by the posterior subdivision of the muscle coincides with loss of the postacetabular iliac process and strong anterior prolongation of the ilium in advanced cynodonts (*14*).

The ITa plesiomorphically ran from the iliac blade dorsal to the acetabulum, but within cynodonts, this origin shifted to lie just anterior to the acetabulum, forming the mammalian RF. This transformation is reflected by a progressive shift in KPs, from anterodorsolaterally oriented to more purely anterior (Fig. 6C). Paralleling the IF, there tends to be a greater dorsal component in more sprawled

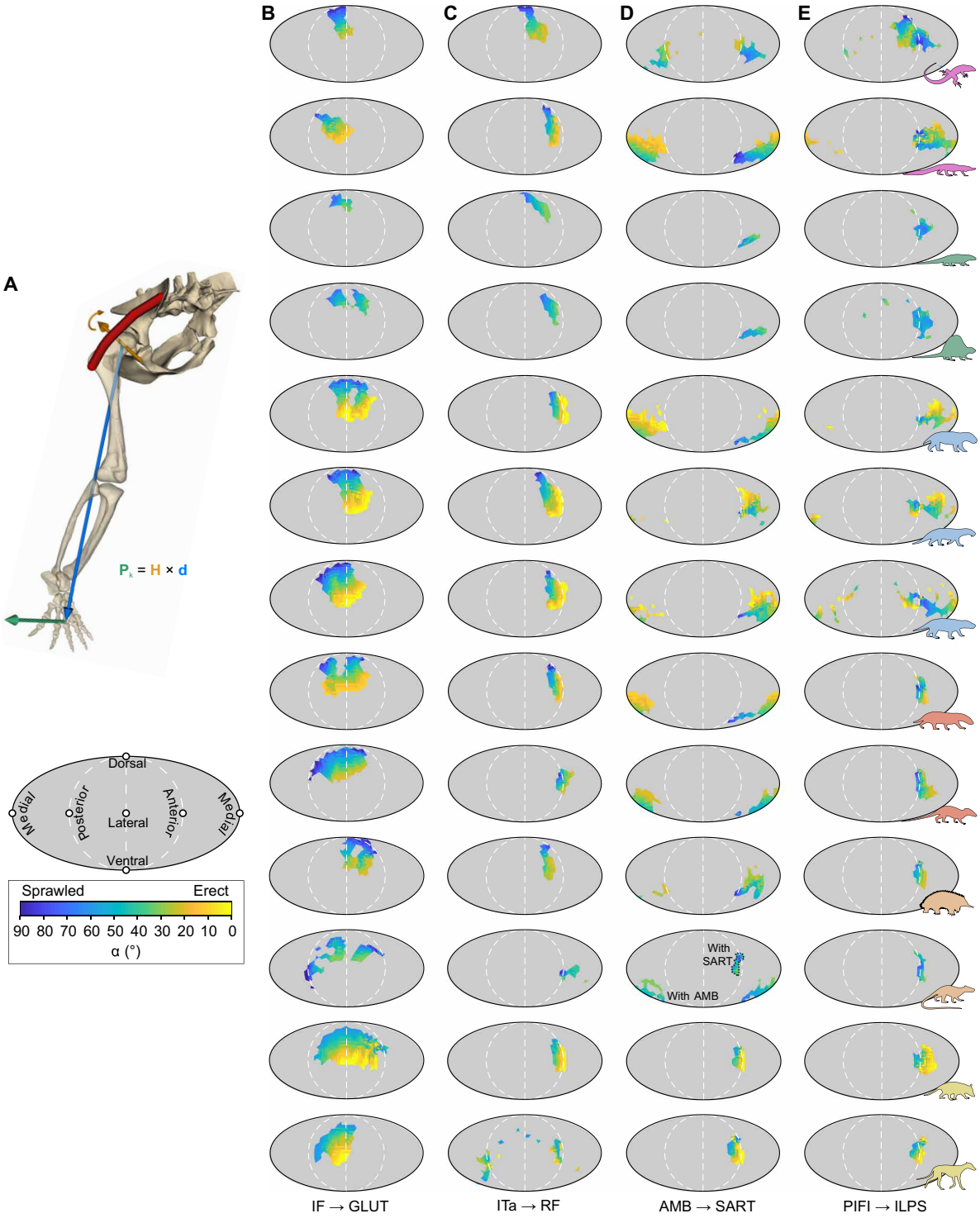

Fig. 6. KPs for major hip muscles. (**A**) Computing muscle KPs, which describe the tendency of a muscle-induced hip joint moment to move the foot in the global reference frame (see Materials and Methods). (**B**) IF/GLUT. (**C**) ITa/RF. (**D**) AMB/SART. (**E**) PIFI/ILPS. Results for osteologically viable postures in each taxon are plotted on a Mollweide projection of the unit sphere and color-coded by adduction angle; results for all subdivisions of a muscle (where relevant) are plotted. In (B) to (E), from top to bottom taxa are *Salvator*, *Alligator*, *Ophiacodon*, *Dimetrodon*, *Oudenodon*, *Lycaenops*, *Regisaurus*, *Massetognathus*, *Megazostrodon*, *Tachyglossus*, *Vincelestes*, *Didelphis*, and *Canis*. See also figs. S3 and S4.

postures. Shifting the origin to lying much closer to the acetabulum also reduced the muscle's potential leverage at the hip, especially in terms of elevation and long-axis rotation (fig. S3B). The effect of hip joint excursion on changes in muscle-tendon length would consequently be reduced, enabling the RF to be more dedicated toward actuation of the knee. Such a functional shift is paralleled by a notable architectural dichotomy among extant taxa (fig. S4C): The ITa of saurians and salamanders is typically parallel fibered or has low pennation, whereas the RF of mammals is markedly pennate, offering greater strength but reduced capacity for length change (*72*). Limited in vivo experimental data for extant tetrapods further highlight this dichotomy, wherein the ITa of salamanders is active principally in swing phase (elevating and protracting the femur) (*73*), but the RF of therians is active principally in stance phase (resisting knee collapse) [e.g., (*74*)]. In vivo data for squamates and crocodylians are currently lacking, but in birds, the anteriormost iliotibialis head, which is parallel fibered and originates anteriorly to and far from the acetabulum, is also primarily active during swing (*75*).

The AMB remained effectively unchanged throughout most of synapsid evolution, running from the base of the pubis toward the knee in pelycosaurs through to monotremes. This conservatism is reflected by ventromedially directed KPs (Fig. 6D) and hip depression moment arms (fig. S3C) in these taxa, which is consistent with a predominantly stance phase activity in squamates (*76*), also observed in the topologically similar pubotibialis in salamanders (*77*). Within stem therians, however, the AMB origin shifted to the anterior ilium, forming the SART. This shift is reflected by KPs focusing tightly in the anterior direction (Fig. 6D) and the muscle becoming a hip elevator and stronger hip protractor, regardless of adduction level (fig. S3C). In turn, extant therians exhibit an altered activity pattern, in which the SART is recruited predominantly or exclusively in the swing phase [e.g., (*71*)], where, because of their erect posture, hip elevation translates principally to limb protraction.

The PIFI plesiomorphically ran from the medial surface of the pubis up to the anterior proximal femur, but on the line to mammals, it transformed to run from the ventral ilium and lumbar vertebrae down to the posteromedial femur, forming the mammalian ILPS. In addition, its insertion on the femur progressively came to occupy the "reptilian" internal trochanter, transforming it into the "mammalian" lesser trochanter (*14*). Despite these major topological shifts, KPs are consistently oriented anteriorly across all taxa and show little correlation with hip adduction (Fig. 6E). This is consonant with the muscle acting predominantly during swing phase across extant tetrapods, serving as a key hip protractor in sprawling taxa or a hip elevator in erect taxa [e.g., (*69*, *70*, *73*, *74*, *75*)], and suggests it to have remained a swing-phase limb protractor throughout synapsid history. However, in stark contrast to this functional conservatism at the whole-limb level, the PIFI's actuation of the hip exhibits multiple shifts between internal and external long-axis rotation throughout synapsid history (fig. S3D). These shifts would have been driven by successive modifications to the muscle's insertion (*14*, *59*), the development of a medially inflected femoral head and neck, and the relative spatial disposition of these features.

DISCUSSION

The transition from sprawling to erect locomotion on the line to modern mammals involved profound changes to musculoskeletal anatomy and limb function, shaped by the constraints imposed by Newtonian mechanics, physiology, and evolutionary contingency, among other factors. Despite an exemplary fossil record, deciphering the temporal sequence and adaptive drivers of these changes has proved difficult. Traditionally, the study of locomotor function in extinct species has largely focused on individual bones, muscles, or joints in isolation [e.g., (*15*–*17*, *20*, *22*, *23*–*25*, *27*, *28*, *40*, *44*–*50*, *78*)], which risks neglecting important interactions that occur between different parts of the body (*39*, *51*), complicating attempts to relate observed anatomical transformation to changes in organismal function, behavior, or ecology. Here, we take a more holistic perspective, viewing musculoskeletal function through the lens of whole-limb performance. Using computational biomechanical modeling to measure a limb's external force-producing capacity (*41*), we apply the concept of an FFS (*39*, *54*) to the fossil record. By quantifying hindlimb performance and muscle function across the sprawling-to-erect transition, we forge stronger links between anatomy, posture, and function throughout synapsid history and explore how major evolutionary shifts in locomotor mechanics may occur.

Evolution of whole-limb performance and posture

The earliest synapsids, the superficially reptilian pelycosaurs, are widely interpreted as having used sprawled postures (*10*, *15*, *22*, *34*, *46*, *68*, *79*), reflecting the plesiomorphic condition inferred for amniotes as a whole. It is therefore not surprising that we found both *Ophiacodon* and *Dimetrodon* to exhibit a sprawling style of hindlimb function (locomotor regime), typified by a more limited range of osteologically viable postures and lower force-producing capacity (Figs. 2 to 4). However, comparison to *Salvator*, especially in terms of FFS volume metrics (Figs. 2 to 4 and fig. S1), suggests that extant squamates may use a hindlimb posture that is more sprawled than that of pelycosaurs and perhaps other early amniotes. This notion is consistent with locomotor patterns inferred for the stem amniote *Orobates* (*42*), the greater emphasis that squamates place on vertebral lateroflexion compared to early and stem amniotes (*33*, *35*), differences in humeral functional morphology between squamates and early amniotes (*15*), and several apomorphies of the hindlimb musculature in saurians, including a hypertrophied, bipartite caudofemoralis muscle (*14*). Evidently, a critical reevaluation of locomotor posture and function in early amniotes is warranted, which can be enhanced through renewed investigation of early sauropsid-line fossils. Irrespective of exactly how the ancestral amniote moved, the origin of mammalian hindlimb function can ultimately trace its roots to a now-lost form of sprawling in pelycosaurs.

Starting from the constrained sprawling locomotor regime of pelycosaurs, a complex history of increasing and decreasing locomotor versatility unfolded across succeeding synapsid grades. Our data indicate increased force-producing capacity in therapsids and basal cynodonts over an extended period of time, before the origin of mammals (Fig. 5 and fig. S2). As a wider range of postures could theoretically be facilitated by higher forces, particularly in many different directions, this result is congruent with the postural flexibility hypothesis for advanced therapsids and cynodonts (*10*, *16*, *40*). Reconstructed magnitudes of several performance metrics for Neotherapsida to Eucynodontia (Fig. 5) are comparable to the magnitudes observed in *Alligator* (Fig. 2), and *Alligator* and *Massetognathus* + therapsids share the most similar performance profiles (Fig. 4B). However, increased hindlimb performance was only temporary, with force-producing capacity in most directions reducing in advanced cynodonts; only posterior force-producing

capacity continues to increase on the line to mammals (Fig. 5A and fig. S2A), suggesting a heightened importance of forward acceleration capacity. The overall reduction in performance parallels a sustained evolutionary reversal toward a less therian-like locomotor regime, initiated in early cynodonts and continued into crown mammals (Fig. 4A). On the basis of current evidence, we conclude that a transient increase in postural or functional versatility in therapsids was not necessarily a prerequisite for the evolution of the erect locomotor regime of crown therians (*16*, *40*): Therians did not directly evolve from a posturally versatile ancestor.

The patterns that collectively typify the extant therians in our study (*Canis* and *Didelphis*) are restricted to just those taxa, distinct from the patterns exhibited by all other taxa (Figs. 2 to 4). We therefore hypothesize that therian-like erect hindlimb function evolved late in synapsid history, probably close to the origin of crown therians themselves. Such a late acquisition reconciles several outstanding issues of the synapsid fossil record. It explains the ectaxonic pedal asymmetry observed in most nontherian synapsids, where digit IV is typically the longest (fig. S5). Marked asymmetry characterizes sprawling squamates and salamanders (*80*, *81*), whereas extant terrestrial therians have broadly symmetric pedes. Similarly, it is consistent with the asymmetry in the knee and ankle joints of most nonmammalian synapsids, which help to orient the pes more anteriorly (fig. S5) (*81*). Our hypothesis is congruent with taphonomic evidence of articulated Mesozoic mammal fossils, wherein nontherians are typically preserved in a dorsoventrally compressed, "spread-eagled" pose (*18*). It is consistent with the retention of a large lesser trochanter in advanced cynodonts and many nontherian mammals, including monotremes [e.g., (*82*, *83*–*86*)]; collision of a large trochanter with the pelvis precludes strongly adducted limb postures in these animals (fig. S6, asterisks). Reduction of the trochanter, coupled with the development of a marked femoral neck (moving the trochanter away from the hip joint), would have been a prerequisite for the evolution of a fully erect posture. Last, our hypothesis is consistent with a dorsally open acetabulum in *Megazostrodon* and *Vincelestes* (*83*, *86*), which would have been poorly suited to buttressing against dorsally directed hip contact forces in adducted postures (fig. S7). When viewed from a whole-limb perspective, the history of synapsid hindlimb locomotor function does not appear to have followed a simple linear transition between sprawling and erect behaviors.

Coevolution of posture and hip muscle function

Our reinterpretation of whole-limb locomotor evolution provides an additional perspective to evaluating the myriad anatomical changes that accompanied the sprawling-to-erect transition in synapsids (Fig. 7). Because of numerous confounding factors, including muscle redundancy and multiarticularity, it is challenging to distill whole-limb force-producing performance into the contributions of individual muscles (*39*, *41*, *51*). Nevertheless, how a given muscle's general action was altered or maintained across such a major functional shift can still be quantified. On the line to mammals, the hindlimb skeleton underwent less structural change compared to that of the forelimb, which involved reconfiguration of the pectoral girdle bones (affording increased mobility of the girdle on the thorax), reorientation of the glenoid, appearance of the sternum, and increased development of muscle attachment processes (*4*, *10*). Despite this, the musculature of the hindlimb underwent greater reorganization compared to that of the forelimb, with certain muscles of the hip in particular undergoing considerable modification (*13*, *14*). Quantifying KPs (Fig. 6) and moment arms (fig. S3) in these muscles allows us to relate anatomical shifts to their global actions and clarify the origin of the distinctive swing- and stance-phase actions of modern therian hindlimb musculature.

Across the four major hip muscle groups studied, we identify three contrasting evolutionary themes.

1) Marked changes in muscle origin can directly lead to functional redeployment, evidenced by both the ITa → RF and AMB → SART. The ITa, plesiomorphically a swing-phase protractor of the hip (Fig. 7A) (*73*), shifted close to the acetabulum in advanced cynodonts to become the RF, becoming geared toward forceful actuation of the knee during stance phase (Fig. 7D) [e.g., (*74*)]. Meanwhile, the AMB, originally acting primarily as a stance-phase hip depressor (Fig. 7A) (*76*, *77*), shifted to the anterior ilium in stem therians to become the SART, elevating the hip during swing phase (Fig. 7E) [e.g., (*71*)]. As hip elevation translates to limb protraction in erect postures, a late transformation of AMB → SART is consistent with a late acquisition of a therian-like erect locomotor regime.

2) Major shifts in function can be realized just by changing posture irrespective of musculoskeletal anatomy, as observed in the IF → GLUT group (Fig. 6B). The IF/GLUT is geared toward swing-phase limb elevation in sprawled poses (*69*, *70*) and stance-phase limb abduction in erect poses [e.g., (*71*)]. That function can be modulated purely by posture cautions against assumptions of the "direction of causality" of IF/GLUT and postural evolution in synapsids [e.g., (*16*, *23*, *25*, *27*, *78*)]; changes in anatomy and muscle recruitment patterns may not be a sole proximate driver of postural evolution but instead a passive consequence of it. As a corollary of a late acquisition of erect hindlimb function within stem therians, we posit the GLUT to act principally during swing phase in extant monotremes, which can be verified by future in vivo study.

3) Global function can be conserved despite major changes to musculoskeletal anatomy and posture, as illustrated by the PIFI → ILPS, which remains a swing-phase limb protractor throughout all of synapsid history (Figs. 6E and 7). Ostensibly, the dorsal-then-anterior shift in origin (*14*, *59*) would have increased its relative length, affording a greater working range and, in turn, enabling faster, larger excursions of the femur during swing. Nevertheless, anatomical changes evidently affected the muscle's actuation of hip long-axis rotation on the line to mammals (fig. S3D).

The juxtaposition of these contrasting themes within a single part of the body is remarkable, as they presumably had to be coordinated with one another to maintain integrated functionality of the hindlimb throughout synapsid locomotor evolution. This is all the more interesting given the repeated shifts in long-axis rotation control by the PIFI, suggesting that various muscles were differentially "taking up the slack" to maintain hip moment balance as posture shifted throughout synapsid history (Fig. 7).

Coordinated evolution of synapsid locomotor function

Beyond clarifying hindlimb functional evolution at the level of both individual muscles and the entire limb, our results can also contribute to an improved understanding of locomotion-related evolutionary changes in other body systems on the line to therians. Given that synapsids remained quadrupedal animals along the therian stem lineage, coordinated evolution between the hindlimb and other parts of the body might well be expected, in order for functional integration to be maintained over time (*2*). In broad agreement with this expectation, the late acquisition of a therian-like erect hindlimb

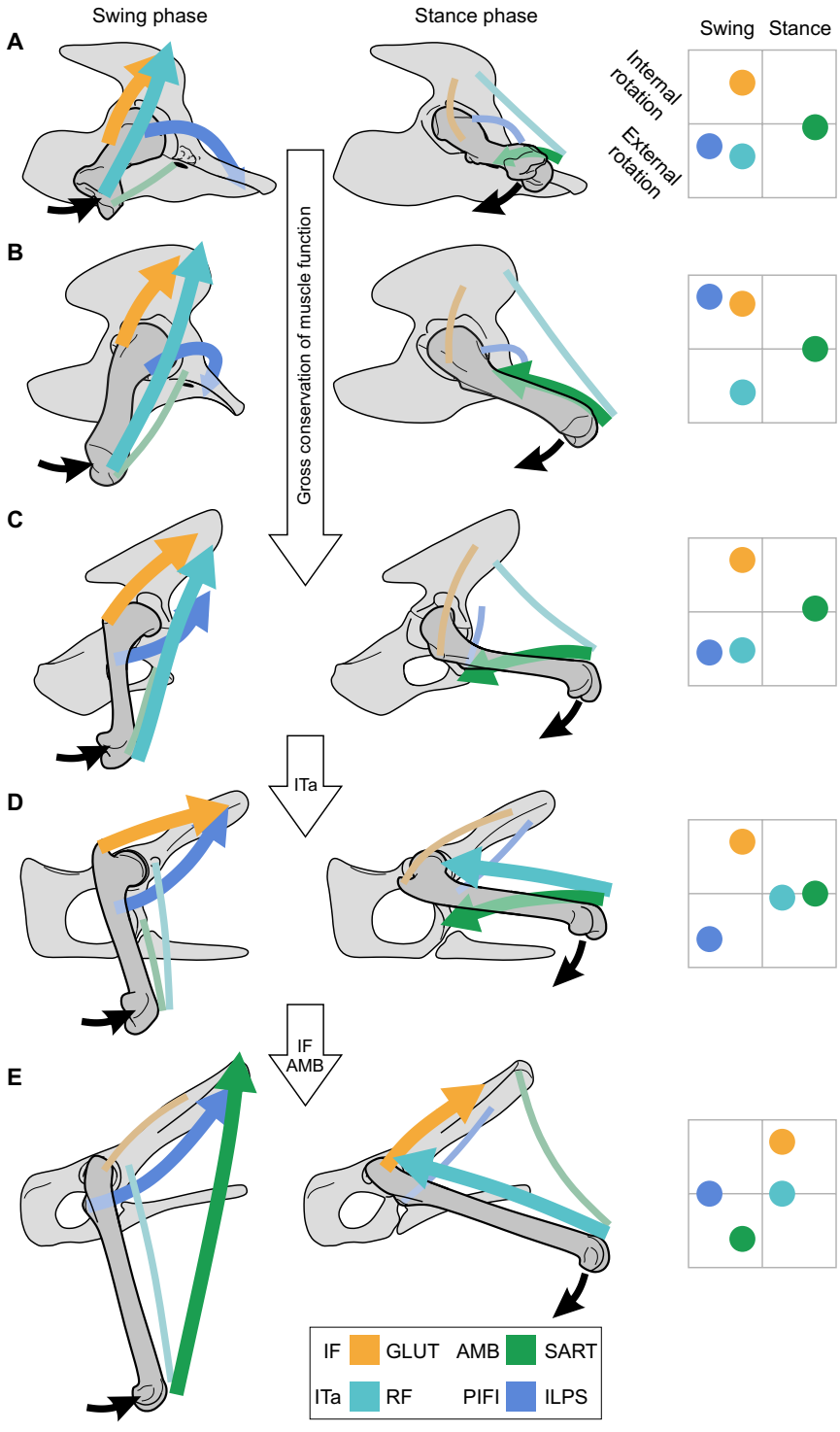

Fig. 7. Hip muscle functional transformation on the line to therians, shown at key stages in synapsid evolution. (**A**) Pelycosaur. (**B**) Therapsid. (**C**) Eucynodont. (**D**) Mammaliamorph. (**E**) Crown therian. Each stage illustrates swing and stance phase; pelvic and femoral dispositions are schematic only. Thick, bright arrows denote when muscles are inferred to be active, and thin, faded lines denote when they are inferred to be inactive; black arrows indicate femoral movement during swing and stance phases. Right column diagrammatically shows actions of each muscle group with respect to hip long-axis rotation (see also fig. S3) in stance and swing, illustrating different combinations of muscles "taking up the slack" in controlling hip long-axis rotation.

function, as hypothesized here, parallels recent evidence of a delayed evolution of the full complement of therian functional traits in the forelimb (*15*) and vertebral column (*33*, *35*). For instance, a fully erect limb posture and enhanced sagittal mobility in the posterior vertebral column appear to have evolved only relatively recently. As both features are linked to asymmetric gaits such as galloping (*55*, *56*), we posit a relatively late origin for these novel gaits within Synapsida. Additional functional analysis of fossil material, especially for stem therians, can provide improved clarity on the precise timing of this characteristically mammalian behavior. Irrespective of when asymmetric gaits evolved, our results for the hindlimb suggest that derived therapsids and cynodonts could well have used similar (and nonerect) fore- and hindlimb postures, offering a resolution to the apparent paradox of prior studies [e.g., (*10*, *16*, *17*, *21*, *22*, *24*, *26*, *27*–*29*)] and reconciling the comparable mediolateral gauge typically observed in fossilized therapsid footprints [e.g., (*87*)]. Dynamic musculoskeletal simulations of whole-animal gait can further evaluate this [e.g., (*88*)].

Although therapsids exhibit indications of evolving toward a therian-like hindlimb locomotor regime, we infer a sustained evolutionary reversal of this trend, commencing around early cynodonts, coupled with an overall reduction in force-generating capacity (Figs. 4 and 5). This reversal in the early cynodont hindlimb coincides with major musculoskeletal reorganization of the forelimb, involving differentiation or migration of multiple muscle masses and restructuring of the scapular blade and humerus toward a more mammalian configuration (*13*, *22*–*24*). However, forelimb function in early cynodonts, as inferred from humeral morphology, does not appear to have markedly changed compared to therapsids, although functional variation and evolutionary lability were increased (*15*). This may suggest a stronger overprint of diversifying ecologies on the forelimb compared to the hindlimb in these animals (*15*). Our taxon sampling is presently relatively coarse, but it is notable that some of these functional changes coincide with the end-Permian mass extinction at ~252 Ma (Fig. 1A) and the subsequent rise to ecological dominance by archosaurs (*89*). It is currently speculative whether ecological marginalization exerted a long-term overprint on locomotor evolution in later cynodonts and early mammals, but is nonetheless an intriguing question deserving future scrutiny.

The transition from sprawling to erect locomotor function on the line to therian mammals was a major theme underlying the rich evolutionary history of Synapsida. By integrating paleontological and anatomical datasets within a physics-based framework, we have shed light on the anatomical and mechanical factors that influenced functional transformation of the synapsid hindlimb. Far from being a simple, linear transition between sprawling and erect end points, our results indicate hitherto unrecognized complexity to the history of whole-limb performance and hip muscle functional reorganization. Although these results support the hypothesis of postural flexibility in advanced therapsids and cynodonts (*10*, *16*, *23*, *40*), we suggest that this flexibility was not critical to the achievement of the erect hindlimb locomotor regime that typifies extant therians. Further, our hypothesis of a late acquisition of erect therian-like hindlimb function contributes to an emerging consilience of evidence that many "classically mammalian" traits probably evolved more recently than traditionally believed. This study reconciles several outstanding problems of the synapsid fossil record and suggests that increased focus on early crown-group mammals is especially warranted in future investigations of locomotor evolution. In addition, as nonerect limb postures engender torsion-heavy bone loading among extant tetrapods [e.g., (*8*, *9*)], our hypothesis implies that many nontherian synapsid fossils may exhibit bone microstructural signatures reflecting this (*90*, *91*), highlighting an additional avenue for further interrogating synapsid locomotor evolution. Using the synapsid hindlimb as an example, we illustrate the value that can be gained from a more holistic, system-level approach to musculoskeletal anatomy, function, and their evolution. Our approach can be applied to a broad diversity of taxa and anatomical systems, and the computational resources that we have developed here will allow future researchers to more thoroughly explore other major functional transitions throughout the history of life.

MATERIALS AND METHODS

Musculoskeletal model creation

We studied five extant taxa that phylogenetically and functionally bracket synapsid locomotor evolution (Table 1): *Salvator merianae*, a sprawled squamate (*61*); *Alligator mississippiensis*, a crocodylian capable of using a range of limb postures (*37*, *38*); *Tachyglossus aculeatus*, a monotreme that uses a sprawled (forelimb) or "semi-erect" (hindlimb) posture (*62*, *63*); *Didelphis virginiana*, a noncursorial erect marsupial (*60*, *63*); and *Canis familiaris*, a cursorial erect placental (*65*, *92*). Eight extinct synapsids were studied, chosen on the basis of accessible, well-preserved, and near-complete fossil material. Collectively, they represent each of the major "grades" of synapsid evolution—pelycosaurs, therapsids, cynodonts, and theriiformes—capturing the main musculoskeletal changes observed during the course of synapsid evolution (*14*, *59*).

Three-dimensional, digital musculoskeletal models of the pelvis and right hindlimb of each taxon were created in OpenSim 3.3 (*43*) following standard protocols (*41*). A detailed description of the model creation process is provided in the Supplementary Materials, and models are provided in data S1. Definition of anatomical and joint coordinate systems broadly followed prior studies (figs. S5 and S8 to S10) (*34*, *93*). In addition to six DOFs used to describe each model's attitude in the global coordinate system, all models had a hip joint with three DOFs and a knee joint with one DOF. Taxonomic variation in distal limb anatomy required different approaches to modeling crural and ankle mobility (see fig. S10 and Supplementary Text). For tractability, the pes was modeled as a single rigid entity, with different approaches taken in defining the ankle joint to account for the disparity in pedal construction and mobility (known or inferred) across taxa. All limb joints were modeled with rotational DOFs only and fixed joint spacing. Although joint translational offsets may affect some lower-level biomechanical metrics, such as joint mobility (*17*, *46*, *48*, *49*, *94*) or muscle moment arms (*52*), these individual effects are expected to diminish at higher levels of anatomical organization, such as whole limbs, when numerous muscles and joints are considered together (*41*). For instance, increases in one muscle's moment arm will correspond with increases for other muscles, including its antagonists, mitigating the net effect; and changes to joint spacing will have minimal impact on whole-limb configurations (i.e., postures) and, in turn, joint moments resulting from applied external forces.

A set of previously reconstructed muscle attachments for each extinct taxon (*59*) was used to guide the creation of muscle-tendon unit (MTU) paths in the models (*41*), also taking into account the topology of musculature (e.g., superficial versus deep and medial versus lateral) observed in extant amniotes. As the ankle joint was

the distalmost joint modeled, the exact location of certain muscle insertions distal to the ankle (e.g., digital flexors) was immaterial. The popliteus and interosseous cruris were only included in *Salvator*, *Tachyglossus*, *Ophiacodon*, and *Dimetrodon*, taxa in which tibiofibular mobility was explicitly modeled. Muscles with an origin inferred to occupy an extensive area of attachment, such as the iliac blade (e.g., IF) or puboischiadic plate (e.g., puboischiofemoralis externus), were represented with two MTUs to account for marked variation in their lines of action (*41*, *52*). Conversely, in extinct taxa where a single muscle may have had multiple subdivisions but supporting evidence is ambiguous, only a single MTU was included. As our reconstructions for extinct taxa involve some uncertainty, we undertook sensitivity analyses to evaluate what effects this may have on our interpretations (see figs. S11 to S13). Overall, we found minimal impact of reconstruction uncertainty on our main results and broader conclusions.

Muscle strengths

Muscles were modeled as a force along a line of action, excluding force-length-velocity relationships. This simplification is necessitated by the great anatomical disparity across species, where estimates of internal architecture, in-series tendon properties, or fiber histochemistry are problematic [e.g., (*41*)]. Thus, only the maximum isometric strength (F_{max}) for each MTU needed to be defined.

For *Canis*, F_{max} was as per the original model (*92*). In *Salvator*, *Tachyglossus*, and *Didelphis*, logistical constraints required muscle strength to be estimated from a second individual for each taxon, using standard muscle architecture dissection techniques. Muscle architecture data for *Salvator* (SEP113, 1.359 kg) and *Didelphis* (SEP102, 1.759 kg) have previously been reported (*58*); data for *Tachyglossus* (SEP48, 3.79 kg) were collected as part of the present study and are reported in data S2. For *Alligator*, muscle architecture data had previously been reported for a similarly sized individual (3.5 kg) (*95*). Maximum isometric strength was calculated as

$$F_{max} = \frac{m_{musc} \cdot \sigma \cdot \cos(\alpha_O)}{\rho \cdot \ell_O} \quad (1)$$

where m_{musc} is muscle belly mass, σ is maximum stress (300,000 N/m^2), α_o is pennation angle at optimum fiber length, ρ is muscle density (1060 kg/m^3), and ℓ_o is optimum fiber length. These values for F_{max} were then scaled to the size of the model by virtue of body mass and assuming isometry (i.e., scaled as mass^{⅔}). As the flexores digitorum longus and brevis were represented by a single compound MTU in the *Didelphis* model, estimated F_{max} values of the two individual muscles were combined in the model. Conversely, as the sheet-like anterior semitendinosus of *Tachyglossus* was represented with two MTUs, estimated F_{max} was split evenly between the two actuators in the model.

Muscle strength is unknowable in extinct species and therefore must be estimated. The great disparity in muscular anatomy across the study taxa (*14*, *59*) obfuscates attempts to rigorously estimate strengths on a per-muscle basis using empirical datasets drawn from extant taxa [e.g., (*41*, *96*)]. However, extinct synapsid limbs would still have been subject to constraints germane to all species, such as muscle packing into a finite volume, which applies across a wide range of extant amniotes (*58*). Irrespective of muscle-specific architecture, total physiological cross-sectional area (and hence F_{max}) across a whole limb or its compartments is strongly correlated with body mass and muscle mass. In this study, we therefore first estimated total limb muscle F_{max} for each extinct taxon (*58*) and then evenly distributed this across the constituent MTUs, deriving an "indirect mean" F_{max}. There are at least two benefits of deriving an estimate of mean F_{max} in this manner, as opposed to a direct estimation of mean F_{max} using similar scaling equations. First, an indirect estimation will be less biased by outliers in the original dataset used to derive the scaling equations (i.e., exceptionally strong or weak muscles). Second, an indirect estimation explicitly accounts for the number of MTUs present in a model—more MTUs equates to lower F_{max} for each MTU—accommodating for uncertainty in reconstructed muscle differentiation. A model reconstructed with more MTUs does not necessarily have greater moment-generating capacity (at a given joint) in and of itself. To examine the reliability of this approach, we undertook sensitivity analyses with the extant taxon models, comparing results between models using dissection-derived and empirically estimated values for F_{max} (see figs. S14 to S16). Despite occasional quantitative differences between strength variants for a given taxon, the qualitative patterns of performance-posture covariation are highly consistent, having little effect on the broader conclusions drawn here.

To derive estimates of F_{max} for each extinct taxon, the original dataset of muscle architecture (*58*) was augmented with the *Tachglossus* measurements and data for *Monodelphis* (*97*). Allometric equations relating body mass (m_{body}) to total F_{max} (in multiples of body weight) were then recalculated (see data S2), for three compartments in the hindlimb:

1) Proximal limb, for muscles whose bulk lies proximal to the knee

$$\log_{10}(\Sigma F_{max}) = -0.28945 \log_{10}(m_{body}) + 1.5836 \quad (2)$$

2) Distal dorsiflexors, for muscles lying distal to the knee and whose principal action is ankle dorsiflexion

$$\log_{10}(\Sigma F_{max}) = -0.30031 \log_{10}(m_{body}) + 0.24133 \quad (3)$$

3) Distal plantarflexors, for the remaining distal muscles

$$\log_{10}(\Sigma F_{max}) = -0.29993 \log_{10}(m_{body}) + 0.91694 \quad (4)$$

To apply these equations, body mass was estimated from the minimal circumferences of the humerus and femur using equation 1 from (*98*) (Table 1). In *Dimetrodon*, *Oudenodon*, *Lycaenops*, *Massetognathus*, *Megazostrodon*, and *Vincelestes*, humeral and femoral circumferences were digitally measured directly from the musculoskeletal model. In *Ophiacodon*, the humerus of FMNH UC 458 was too fragmentary for reliable measurement, so humeral circumference was based on MCZ VPRA-1486 (*15*), its mesh model being isometrically scaled to the dimensions of FMNH UC 458 by virtue of proximodistal length before diaphyseal circumference was measured. In *Regisaurus*, the humerus is not preserved in BP/1/5394. Thus, two other eutherocephalian specimens with complete femora and humeri were referred to, namely BP/1/3973 *Olivierosuchus parringtoni* and UMZC T.837 *Scaloposaurus constrictus*; on the basis of the ratio of femoral to humeral circumference in these specimens, humeral circumference was estimated for *Regisaurus*. Body mass as estimated here is similar to a previous estimate for the same specimen based on glenoid area (*40*). Although stylopod

circumferences may produce problematic estimates for some non-mammalian synapsids [e.g., (*29*)], our approach to expressing performance relative to muscle strength (see below) means that assessments of performance are largely unaffected by potential error in body mass.

Performance, posture, and body size

We developed a pipeline for rapidly computing high-fidelity FFSs, integrating the OpenSim modeling framework with an optimization approach (*99*) in MATLAB (v9.5, MathWorks, USA; see the Supplementary Materials and data S3). This method leverages Newton's third law, seeking the maximum magnitude of externally applied end-point force (in a given direction) for which external moments at each limb joint can still be balanced internally by muscles (*41*). Maximum forces are able to be calculated for a large number of directions (fig. S17) rapidly, and for which hip joint contact forces respect acetabular geometry (see fig. S18 and Supplementary Text). As FFSs are a global property of the limb, their computation and analysis are independent of the joint coordinate systems, reference pose, or rotation conventions used in a musculoskeletal model, unlike moment arms [e.g., (*100*)]. In this study, we focus on two aspects of the FFS to quantify locomotor performance in the global context of the external environment, both measured in newtons: first, the magnitude of force in each of the cardinal directions, that is, ventral, dorsal, anterior, posterior, medial, and lateral; and, second, the CRV and how this is partitioned into different directions, that is, ventral versus dorsal, anterior versus posterior, and medial versus lateral (Fig. 1B). The second set of metrics is less intuitive but can be interpreted as indicators of overall force-producing capacity, accounting for all possible directions at once (*39*). Because of their quasi-convex geometry (*54*), greater FFS volumes are more readily achieved by sustained force production across a wide range of directions (i.e., higher directional versatility in force production), rather than high force production in a narrow band of directions.

A limb's force-producing capacity can vary considerably with posture [e.g., (*41*, *54*, *57*)]. Thus, for each of our taxa, FFSs were computed for many postures spanning a continuum of whole-limb adduction, flexion, and forward-backward pitch of the whole limb at the hip joint (Fig. 1, C and D, and see also data S1); pelvic orientation was fixed in its reference pose, with only the configuration of the limb itself varied. Postures were standardized to facilitate comparison across taxa of different limb proportions. First, a "base set" of postures was generated, where the limb end point was located purely lateral to the hip, that is, in a coronal plane passing through the acetabulae, and where the pes pointed forward as practically as possible. We set the end point at the center of the distal metatarsus (*101*), placing it close to the middle of the pes; this approximates the location of the center of pressure during stance phase and avoids complications introduced by marked interspecific variation in relative digit length. Three levels of whole-limb flexion were tested, where end point–hip distance was set at a fixed proportion of end point–hip distance in the model's reference pose (L_{ref}; Fig. 1C, fig. S9, and movie S1): $0.5 \times L_{ref}$ defined "crouched," $0.7 \times L_{ref}$ defined "intermediate," and $0.9 \times L_{ref}$ defined "extended." Within each level of limb flexion was a range of postures spanning different levels of limb adduction. Here, we use hip adduction angle as a measure of how sprawled or erect a given posture is, defined as the smallest angle between the femoral long axis and the sagittal plane of the pelvis' frame of reference (Fig. 1C) (*7*). It may be calculated from the Euler angles used to explicitly describe hip attitude as

$$\alpha = arcsin\left(cos\theta_y cos\theta_z\right) \quad (5)$$

where θ_z and θ_y denote protraction-retraction and elevation-depression angles, respectively [cf. (*34*)] (see also the Supplementary Materials). Postures spanned fixed 10° increments of adduction angle, from $\alpha = 0°$ (fully erect) to $\alpha = 90°$ (fully sprawled).

Individual postures were generated in OpenSim following an inverse kinematics approach. Here, we sought to derive postures that satisfied the constraints of (i) a given adduction angle, (ii) a given end point–hip distance, (iii) the pes facing forward as practically as possible, and (iv) the ankle situated at the same level or higher than the distal metatarsus. Working within these constraints, limb posture was straightforward to derive; for consistency, joint angles were modified in a hierarchical order, starting with hip protraction-retraction and elevation-depression (covaried according to adduction angle), followed by hip long-axis rotation and then by knee, crus (if applicable), and ankle angles. The resulting postures within a given level of whole-limb flexion varied smoothly, usually monotonically, with respect to limb adduction (Fig. 1C, movie S1, and data S1). With 10 levels of adduction and 3 levels of whole-limb flexion, a total of 30 base postures potentially exist for each model (Fig. 1C). However, segment proportions and joint axis orientation reduced the number of feasible postures to 18 to 27 depending on the taxon. These postures comprise what is kinematically feasible only; whether a given posture was osteologically viable (i.e., respected bony and articular geometry; see fig. S6) was only considered after calculation. Once we generated the base set of postures, these were pitched about the global mediolateral axis at the hip by 15° posteriorly and 15° and 30° anteriorly (Fig. 1D; affecting hip angles only). The broader range of postures better reflects the fact that tetrapod hindlimbs can generate considerable forces when the feet are anterior or posterior to the hip, not just lateral to it. A grand total of 72 to 108 postures were tested for each taxon.

Empirical contextualization

Experimentally measuring a limb's maximal force-generating capacity in all directions is not practical in animals [but see (*102*) for a robotic example], highlighting the powerful, complementary benefit that FFS analysis can provide to understanding limb function. To integrate our analytical results within an empirical framework, we identified "habitual" postures used during steady-state terrestrial locomotion in each extant taxon (Fig. 2 and fig. S1, yellow bars), enabling an assessment of which force performance metrics contain important correlative signal of locomotor posture (kinematics). These postures are defined as the hip adduction angles that most closely correspond to those used around mid-stance of steady locomotion, as reported by prior in vivo experimental studies. For *Salvator*, this was based on (*61*, *64*); for *Alligator*, this was based on sprawled and high-walk postures recorded in (*38*); for *Didelphis*, this was based on (*63*, *64*); and for *Canis*, this was based on data for whippets collected in (*65*). For *Tachyglossus*, this was based on (*62*, *63*), although it should be noted that dorsal and lateral views of the skeleton were recorded separately in those studies (i.e., not a truly three-dimensional assessment). These habitual postures provide a useful starting point for investigating how FFSs reflect realized limb function during locomotion. Nonetheless, these are an incomplete excerpt of in vivo locomotor posture, since a range

of limb postures are used throughout gait, and even wider range across an animal's full locomotor repertoire.

Size normalization

As the taxa studied here span an estimated 2500-fold range in body mass (Table 1), this needs to be accounted for in interspecific comparisons of performance. Metrics of force production are typically normalized to multiples of body weight to express performance in the context of support or propulsion of the individual. However, such an approach is inadequate if the goal is to assess how internal muscular forces are converted to external forces on the environment, as is the case here, because it does not account for negative allometry in muscle strength with increasing body size [e.g., (*58*)]. All else being equal, an 88-kg *Ophiacodon* should have lower relative force-producing capacity than a 35-g *Megazostrodon*, simply by virtue of being a larger animal. We therefore used an alternative approach to accounting for size, by first computing a given model's "intrinsic strength" as the average F_{max} of all MTUs present. Size-normalized limb force production was then determined by dividing a given FFS metric F_i by this model-specific intrinsic strength

$$F_i^* = \frac{F_i}{\frac{1}{N}\sum_{j}^{N} F_{\max,j}} \tag{6}$$

where N is the number of MTUs in the model. The resulting normalized metric, expressed in dimensionless MSUs, implicitly factors in body size by accounting for muscle allometry in the derivation of the model's intrinsic strength. Analogous to the concept of mechanical advantage in a lever system, this normalization describes how much external environmental force is generated per unit muscle force, thus permitting fairer interspecific comparisons in the context of the underlying musculoskeletal anatomy only, such as bone and segment proportions, joint axis orientations, muscle attachments, and muscle subdivisions.

Locomotor performance profiles

To comprehensively characterize the similarity and contrast between each taxon's FFS results, we defined the performance profile of each taxon by constructing a matrix of results for every performance metric, at every level of adduction, flexion, and pitch, for a total of $13 \times 10 \times 3 \times 4 = 1560$ entries per taxon (see data S3). For postures that were not kinematically feasible and osteologically viable, the corresponding entry for each performance metric was set to zero. These matrices are a collective measure of locomotor function in each taxon. To focus on how patterns, rather than absolute performance, compared across taxa, values in each matrix were normalized by the maximum attained magnitude in each metric for a given taxon. We then characterized how therian-like each taxon's performance profile is by calculating the pairwise Pearson correlation between its matrix and the matrix for *Canis* (using *Didelphis* as the reference taxon instead produced nearly identical results). To provide a reference-agnostic assessment of similarity and contrast across taxa, we also ran an agglomerative hierarchical cluster analysis of the performance matrices, using Ward's linkage method.

Evolution of hindlimb performance

To explore the evolution of hindlimb performance, we ran ancestral state reconstructions of each performance metric individually using maximum likelihood and assuming a Brownian motion model of evolution, using the "ape" (v5.6-2; (*103*) and "phytools" (v1.2-0) (*104*) packages for R (v4.1.0) (*105*). Our time-calibrated phylogenetic tree (Fig. 1A) was based on ages extracted from the Paleobiology Database (*106*). To assess whether a given performance metric changed significantly through time, reconstructed nodal values were regressed against nodal ages using the "stepAIC" function of the "MASS" package (v7.3-54 (*107*), testing linear and quadratic terms. As these assessments may be sensitive to our approach to representing performance with a singular snapshot and more broadly other modeling assumptions (e.g., estimates of muscle strength), we performed our reconstructions within a Monte Carlo simulation framework. A total of 1000 replicates were run, whereby the original value for each performance metric for each taxon was randomly perturbed by up to 20%, drawing from a uniform distribution. All code and necessary files are provided in data S4.

Hip muscle KPs

We also sought to assess the potential contributions of hip muscles to whole-limb function, irrespective of the modulating effects of other muscles. Given an MTU's geometry with respect to a focal joint (i.e., origin, insertion, and line of action), its action at that joint can be expressed in a global context by computing its potential to effect movement of the limb end point, which we term its KP (Fig. 6A). This potential is calculated assuming that all other joints are fixed, by computing the cross product of the MTU's net hip joint moment vector $\mathbf{H}$ (for an applied muscle force of 1 N) and the limb's end-point vector $\mathbf{d}$ (i.e., distance vector from the hip joint to the limb end point)

$$\mathbf{P}_k = \mathbf{H} \times \mathbf{d} \tag{7}$$

As limb posture can alter $\mathbf{H}$ (via hip muscle moment arms) and $\mathbf{d}$, KPs will therefore vary with posture. In describing the tendency of $\mathbf{H}$ to move the end point in a particular direction in the global reference frame, a KP is independent of the joint coordinate system, reference pose, or rotation convention used. In this study, we focus on variation in its directional component only (as a unit vector), which provides a tangible expression of how moment arms with respect to different anatomical axes covary with each other and posture in a given muscle. This geometric approach avoids the complexity inherent to an analysis of all muscles together, where, because of redundancy, different muscle activation patterns result in different kinematics of the end point (*101*). See data S3 for code used to execute the calculations.

Supplementary Materials

The PDF file includes:

Supplementary Text
Figs. S1 to S19
Legend for movie S1
References

Other Supplementary Material for this manuscript includes the following:

Movie S1

REFERENCES AND NOTES

1. K. P. Dial, N. H. Shubin, E. L. Brainerd, *Great Transformations in Vertebrate Evolution* (Univ. of Chicago Press, 2015).
2. T. S. Kemp, *The Origin of Higher Taxa* (Oxford Univ. Press, 2015).
3. P. D. Polly, in *Fins into Limbs: Evolution, Development, and Transformation*, B. K. Hall, Ed. (Univ. of Chicago Press, 2007).

4. T. S. Kemp, *The Origin and Evolution of Mammals* (Oxford Univ. Press, Oxford, 2004).
5. J. Gray, *Animal Locomotion* (William Cloes and Sons Ltd, 1968).
6. F. A. Jenkins Jr., G. E. Goslow Jr., The functional anatomy of the shoulder of the savannah monitor lizard (*Varanus exanthematicus*). *J. Morphol.* **175**, 195–216 (1983).
7. J. R. Hutchinson, S. M. Gatesy, Adductors, abductors, and the evolution of archosaur locomotion. *Paleobiology* **26**, 734–751 (2000).
8. R. W. Blob, A. A. Biewener, *In vivo* locomotor strain in the hindlimb bones of *Alligator mississippiensis* and *Iguana iguana*: Implications for the evolution of limb bone safety factor and non-sprawling limb posture. *J. Exp. Biol.* **202**, 1023–1046 (1999).
9. K. M. Sheffield, R. W. Blob, Loading mechanics of the femur in tiger salamanders (*Ambystoma tigrinum*) during terrestrial locomotion. *J. Exp. Biol.* **214**, 2603–2615 (2011).
10. T. S. Kemp, *Mammal-like Reptiles and the Origin of Mammals* (Academic Press, 1982).
11. K. E. Jones, K. D. Angielczyk, P. D. Polly, J. J. Head, V. Fernandez, J. K. Lungmus, S. Tulga, S. E. Pierce, Fossils reveal the complex evolutionary history of the mammalian regionalized spine. *Science* **361**, 1249–1252 (2018).
12. J. K. Lungmus, K. D. Angielczyk, Antiquity of forelimb ecomorphological diversity in the mammalian stem lineage (Synapsida). *Proc. Natl. Acad. Sci. U.S.A.* **116**, 6903–6907 (2019).
13. P. J. Bishop, S. E. Pierce, The fossil record of appendicular muscle evolution in Synapsida on the line to mammals: Part I – Forelimb. *Anat. Rec.* **307**, 1764–1825 (2024).
14. P. J. Bishop, S. E. Pierce, The fossil record of appendicular muscle evolution in Synapsida on the line to mammals: Part II – Hindlimb. *Anat. Rec.* **307**, 1826–1896 (2024).
15. R. J. Brocklehurst, M. Mercado, K. D. Angielczyk, S. E. Pierce, Adaptive landscapes unveil the complex evolutionary path to mammalian forelimb function and posture. bioRxiv 2024.03.12.584484 (Preprint) (2024). http://dx.doi.org/10.1101/2024.03.12.584484.
16. T. S. Kemp, Stance and gait in the hindlimb of a therocephalian mammal-like reptile. *J. Zool.* **186**, 143–161 (1978).
17. P. H. Lai, A. A. Biewener, S. E. Pierce, Three-dimensional mobility and muscle attachments in the pectoral limb of the Triassic cynodont *Massetognathus pascuali* (Romer, 1967). *J. Anat.* **232**, 383–406 (2018).
18. Z. Kielan-Jaworowska, J. H. Hurum, Limb posture in early mammals: Sprawling or parasagittal. *Acta Palaeontol. Pol.* **51**, 393–406 (2006).
19. G. Li, Z.-X. Luo, A Cretaceous symmetrodont therian with some monotreme-like postcranial features. *Nature* **439**, 195–200 (2006).
20. J. Fröbisch, Locomotion in derived dicynodonts (Synapsida, Anomodontia): A functional analysis of the pelvic girdle and hind limb of *Tetragonias njalilus*. *Can. J. Earth Sci.* **43**, 1297–1308 (2006).
21. M. L. Guignard, A. G. Martinelli, M. B. Soares, Reassessment of the postcranial anatomy of *Prozostrodon brasiliensis* and implications for postural evolution of non-mamaliaform cynodonts. *J. Vertebr. Paleontol.* **38**, e1511570 (2018).
22. F. A. Jenkins Jr., The Postcranial Skeleton of African Cynodonts Bull. Peabody Mus. Nat. Hist. 36, 1–216 (1971).
23. T. S. Kemp, The primitive cynodont *Procynosuchus*: Structure, function and evolution of the postcranial skeleton. *Philos. Trans. R. Soc. B* **288**, 217–258 (1980).
24. T. S. Kemp, Aspects of the structure and functional anatomy of the Middle Triassic cynodont *Luangwa*. *J. Zool.* **191**, 193–239 (1980).
25. C. Sullivan, J. Liu, E. M. Roberts, T. D. Huang, C. Yang, S. Zhong, Pelvic morphology of a tritylodontid (Synapsida: Eucynodontia) from the Lower Jurassic of China, and some functional and phylogenetic implications. *C. R. Palevol* **12**, 505–518 (2013).
26. F. A. Jenkins Jr., The Chañares (Argentina) Triassic reptile fauna VII. The postcranial skeleton of the traversodontid *Massetognathus pascuali* (Therapsida, Cynodontia). *Breviora* **352**, 1–28 (1970).
27. G. M. King, The functional anatomy of a Permian dicynodont. *Philos. Trans. R. Soc. B* **291**, 243–322 (1981).
28. S. Ray, A. Chinsamy, Functional aspects of the postcranial anatomy of the Permian Dicynodont *Diictodon* and their ecological implications. *Palaeontology* **46**, 151–183 (2003).
29. M. Romano, B. S. Rubidge, First 3D reconstruction and volumetric body mass estimate of the tapinocephalid dinocephalian *Tapinocaninus pamelae* (Synapsida: Therapsida). *Hist. Biol.* **33**, 498–505 (2021).
30. F. A. Jenkins Jr., The functional anatomy and evolution of the mammalian humero-ulnar articulation. *Am. J. Anat.* **137**, 281–298 (1973).
31. K. E. Jones, K. D. Angielczyk, S. E. Pierce, Stepwise shifts underlie evolutionary trends in morphological complexity of the mammalian vertebral column. *Nat. Commun.* **10**, 5071 (2019).
32. K. E. Jones, S. Gonzalez, K. D. Angielczyk, S. E. Pierce, Regionalization of the axial skeleton predates functional adaptation in the forerunners of mammals. *Nat. Ecol. Evol.* **4**, 470–478 (2020).
33. K. E. Jones, B. V. Dickson, K. D. Angielczyk, S. E. Pierce, Adaptive landscapes challenge "lateral-to-sagittal" paradigm for mammalian vertebral evolution. *Curr. Biol.* **31**, 1883–1892.e7 (2021).
34. R. J. Brocklehurst, P. Fahn-Lai, S. Regnault, S. E. Pierce, Musculoskeletal modeling of sprawling and parasagittal forelimbs provides insight into synapsid postural transition. *iScience* **25**, 103578 (2022).
35. K. E. Jones, K. D. Angielczyk, S. E. Pierce, Origins of mammalian vertebral function revealed through digital bending experiments. *Proc. Biol. Sci.* **291**, 20240820 (2024).
36. T. S. Kemp, in *Principles of Construction in Fossil and Recent Reptiles*, J. Reiss, E. Frey, Eds. (University of Stuttgart and University of Tübingen, 1985), pp. 181–191.
37. S. M. Gatesy, Hind limb movements of the American alligator (*Alligator mississippiensis*) and postural grades. *J. Zool.* **224**, 577–588 (1991).
38. H. P. Tsai, M. L. Turner, A. R. Manafzadeh, S. M. Gatesy, Contrast-enhanced XROMM reveals *in vivo* soft tissue interactions in the hip of *Alligator mississippiensis*. *J. Anat.* **236**, 288–304 (2020).
39. F. J. Valero-Cuevas, *Fundamentals of Neuromechanics* (Springer-Verlag, 2016).
40. R. W. Blob, Evolution of hindlimb posture in nonmammalian therapsids: Biomechanical tests of paleontological hypotheses. *Paleobiology* **27**, 14–38 (2001).
41. P. J. Bishop, A. R. Cuff, J. R. Hutchinson, How to build a dinosaur: Musculoskeletal modeling and simulation of locomotor biomechanics in extinct animals. *Paleobiology* **47**, 1–38 (2021).
42. J. A. Nyakatura, K. Melo, T. Horvat, K. Karakasiliotis, V. R. Allen, A. Andikfar, E. Andrada, P. Arnold, J. Lauströer, J. R. Hutchinson, M. S. Fischer, A. J. Ijspeert, Reverse-engineering the locomotion of a stem amniote. *Nature* **565**, 351–355 (2019).
43. A. Seth, J. L. Hicks, T. K. Uchida, A. Habib, C. L. Dembia, J. J. Dunne, C. F. Ong, M. S. DeMers, A. Rajagopal, M. Millard, S. R. Hamner, E. M. Arnold, J. R. Yong, S. K. Lakshmikanth, M. A. Sherman, J. P. Ku, S. L. Delp, OpenSim: Simulating musculoskeletal dynamics and neuromuscular control to study human and animal movement. *PLOS Comput. Biol.* **14**, e1006223 (2018).
44. S. C. R. Maidment, K. T. Bates, P. L. Falkingham, C. VanBuren, V. Arbour, P. M. Barrett, Locomotion in ornithischian dinosaurs: An assessment using three-dimensional computational modelling. *Biol. Rev.* **89**, 588–617 (2014).
45. T. V. De Oliveira, C. L. Schultz, Functional morphology and biomechanics of the cynodont *Trucidocynodon riograndensis* from the Triassic of Souther Brazil: Pectoral girdle and forelimb. *Acta Palaeontol. Pol.* **61**, 377–386 (2015).
46. P. J. Bishop, R. J. Brocklehurst, S. E. Pierce, Intelligent sampling of high-dimensional joint mobility space for analysis of articular function. *Methods Ecol. Evol.* **14**, 569–582 (2023).
47. M. Dempsey, S. C. R. Maidment, B. P. Hedrick, K. T. Bates, Convergent evolution of quadrupedality in ornithischian dinosaurs was achieved through disparate forelimb muscle mechanics. *Proc. Biol. Sci.* **290**, 20222435 (2023).
48. E. C. Herbst, A. R. Manafzadeh, J. R. Hutchinson, Multi-joint analysis of pose viability supports the possibility of salamander-like hindlimb configurations in the Permian tetrapod *Eryops megacephalus*. *Integr. Comp. Biol.* **62**, 139–151 (2022).
49. O. E. Demuth, E. J. Rayfield, J. R. Hutchinson, 3D hindlimb biomechanics of the stem-archosaur *Euparkeria capensis* with implications for postural evolution within Archosauria. *Sci. Rep.* **10**, 15357 (2020).
50. J. L. Molnar, J. R. Hutchinson, R. Diogo, J. A. Clack, S. E. Pierce, Evolution of forelimb musculoskeletal function across the fish-to-tetrapod transition. *Sci. Adv.* **7**, eabd7457 (2021).
51. A. D. Kuo, in *Classics in Movement Science*, M. L. Latash, V. M. Zatsiorsky, Eds. (Human Kinetics, 2001), pp. 289–315.
52. C. A. Brassey, S. C. R. Maidment, P. M. Barrett, Muscle moment arm analyses applied to vertebrate paleontology: A case study using *Stegosaurus stenops* Marsh, 1887. *J. Vertebr. Paleontol.* **37**, e1361432 (2017).
53. S. Regnault, S. E. Pierce, Pectoral girdle and forelimb musculoskeletal function in the echidna (*Tachyglossus aculeatus*): Insights into mammalian locomotor evolution. *R. Soc. Open Sci.* **5**, 181400 (2018).
54. F. J. Valero-Cuevas, in *Progress in Motor Control – A Multidisciplinary Perspective*, D. Sternad, Ed. (Springer, 2009), pp. 619–633.
55. R. M. Alexander, *Principles of Animal Locomotion* (Princeton Univ. Press, 2006).
56. A. A. Biewener, S. N. Patek, *Animal Locomotion* (Oxford Univ. Press, ed. 2, 2018).
57. H. X. Hoang, J. A. Reinbolt, Crouched posture maximizes ground reaction forces generated by muscles. *Gait Posture* **36**, 405–408 (2012).
58. P. J. Bishop, M. A. Wright, S. E. Pierce, Whole-limb scaling of muscle mass and force-generating capacity in amniotes. *PeerJ* **9**, e12574 (2021).
59. P. J. Bishop, S. E. Pierce, Reconstructions of hindlimb musculature in extinct pre-therian synapsids. *Bull. Mus. Comp. Zool.* **163**, 417–471 (2024).
60. W. C. Gosnell, M. T. Butcher, T. Maie, R. W. Blob, Femoral loading mechanics in the Virginia opossum, *Didelphis virginiana*: Torsion and mediolateral bending in mammalian locomotion. *J. Exp. Biol.* **214**, 3455–3466 (2011).
61. K. M. Sheffield, M. T. Butcher, S. K. Shugart, J. C. Gander, R. W. Blob, Locomotor loading mechanics in the hindlimbs of tegu lizards (*Tupinambis merianae*): Comparative and evolutionary implications. *J. Exp. Biol.* **214**, 2616–2630 (2011).
62. F. A. Jenkins Jr., Limb movements in a monotreme (*Tachyglossus aculeatus*): A cineradiographic analysis. *Science* **168**, 1473–1475 (1970).
63. F. A. Jenkins Jr., Limb posture and locomotion in the Virginia opossum (*Didelphis virginiana*) and in other non-cursorial mammals. *J. Zool.* **165**, 303–315 (1971).
64. P. Fahn-Lai, "Shoulder to shoulder: Musculoskeletal function of the amniote pectoral girdle and the foundations of the mammalian forelimb," thesis, Harvard University (2021).

65. M. S. Fischer, S. V. Lehmann, E. Andrada, Three-dimensional kinematics of canine hind limbs: In vivo, biplanar, high-frequency fluoroscopic analysis of four breeds during walking and trotting. *Sci. Rep.* **8**, 16982 (2018).
66. D. L. Jindrich, M. Qiao, Maneuvers during legged locomotion. *Chaos* **19**, 026105 (2009).
67. D. L. Jindrich, R. J. Full, Many-legged maneuverability: Dynamics of turning in hexapods. *J. Exp. Biol.* **202**, 1603–1623 (1999).
68. J. A. Hopson, in *Great Transformations in Vertebrate Evolution,* K. P. Dial, N. H. Shubin, E. L. Brainerd, Eds. (University of Chicago Press, 2015), pp. 125–141.
69. T. J. M. Dick, C. J. Clemente, How to build your dragon: Scaling of muscle architecture from the world's smallest to the world's largest monitor lizard. *Front. Zool.* **13**, 8 (2016).
70. S. M. Gatesy, An electromyographic analysis of hindlimb function in *Alligator* during terrestrial locomotion. *J. Morphol.* **234**, 197–212 (1997).
71. G. E. Goslow Jr., H. J. Seeherman, C. R. Taylor, M. N. McCutchin, N. C. Heglund, Electrical activity and relative length changes of dog limb muscles as a function of speed and gait. *J. Exp. Biol.* **94**, 15–42 (1981).
72. A. Wilson, G. Lichtwark, The anatomical arrangement of muscle and tendon enhances limb versatility and locomotor performance. *Philos. Trans. R. Soc. B* **366**, 1540–1553 (2011).
73. S. E. Pierce, L. P. Lamas, L. Pelligand, N. Schilling, J. R. Hutchinson, Patterns of limb and epaxial muscle activity during walking in the fire salamander, *Salamandra salamandra*. *Integr. Org. Biol.* **2**, obaa015 (2020).
74. S. Nicolopoulos-Stournaras, J. F. Iles, Hindlimb muscle activity during locomotion in the rat (*Rattus norvegicus*) (Rodentia: Muridae). *J. Zool.* **203**, 427–440 (1984).
75. S. M. Gatesy, Guineafowl hindlimb function II: Electromyographic analysis and motor pattern evolution. *J. Morphol.* **240**, 127–142 (1999).
76. K. L. Foster, T. E. Higham, Context-dependent changes in motor control and kinematics during locomotion: Modulation and decoupling. *Proc. Biol. Sci.* **281**, 20133331 (2014).
77. M. A. Ashley-Ross, Patterns of hind limb motor output during walking in the salamander *Dicamptodon tenebrosus*, with compariusons to other tetrapods. *J. Comp. Physiol. A* **177**, 273–285 (1995).
78. A. S. Romer, The Locomotor Apparatus of Certain Primitive and Mammal-Like Reptiles. Bull. Am. Mus. Nat. Hist. 46, 517–606 (1922).
79. A. S. Romer, L. I. Price, *Review of the Pelycosauria* (Geological Society of America, 1940).
80. E. T. B. Francis, *The Anatomy of the Salamander* (Oxford Univ. Press, 1934).
81. S. C. Rewcastle, Fundamental adaptations in the lacertilian hind limb: A partial analysis of the sprawling limb posture and gait. *Copeia* **1983**, 476–487 (1983).
82. W. G. Kühne, *The Liassic Therapsid Oligokyphus* (British Museum (Natural History), 1956).
83. F. A. Jenkins Jr., F. R. Parrington, The postcranial skeletons of the Triassic mammals *Eozostrodon*, *Megazostrodon* and *Erythrotherium*. *Philos. Trans. R. Soc. B* **273**, 387–431 (1976).
84. F. A. Jenkins Jr., C. R. Schaff, The Early Cretaceous mammal *Gobiconodon* (Mammalia, Triconodonta) from the Cloverly Formation in Montana. *J. Vertebr. Paleont.* **8**, 1–24 (1988).
85. K. R. K. Jäger, Z.-X. Luo, T. Martin, Postcranial skeleton of *Henkelotherium guimarotae* (Cladotheria, Mammalia) and locomotor adaptation. *J. Mamm. Evol.* **27**, 349–372 (2019).
86. G. W. Rougier, "*Vincelestes neuquenianus* Bonaparte (Mammalia, Theria) un primitivo mamifero del Cretacio Inferior de la Cuenca Neuquina," thesis, Universidad Nacional de Buenos Aires (1993).
87. L. Marchetti, H. Klein, M. Buchwitz, A. Ronchi, R. M. H. Smith, W. J. de Klerk, L. Sciscio, G. H. Groenewald, Permian-Triassic vertebrate footprints from South Africa: Ichnotaxonomy, producers and biostratigraphy through two major faunal crises. *Gondw. Res.* **72**, 139–168 (2019).
88. P. J. Bishop, A. Falisse, F. De Groote, J. R. Hutchinson, Predictive simulations of running gait reveal a critical dynamic role of the tail in bipedal dinosaur locomotion. *Sci. Adv.* **7**, eabi7348 (2021).
89. H.-D. Sues, N. C. Fraser, *Triassic Life on Land: The Great Transition* (Columbia Univ. Press, 2010).
90. P. J. Bishop, S. A. Hocknull, C. J. Clemente, J. R. Hutchinson, A. A. Farke, B. R. Beck, R. S. Barrett, D. G. Lloyd, Cancellous bone architecture and theropod dinosaur locomotion. Part I – An examination of cancellous bone architecture in the hindlimb bones of theropods. *PeerJ* **6**, e5778 (2018).
91. E. de Margerie, S. Sanchez, J. Cubo, J. Castanet, Torsional resistance as a principal component of the structural design of long bones: Comparative multivariate evidence in birds. *Anat. Rec.* **282A**, 49–66 (2005).
92. R. G. Ellis, J. W. Rankin, J. R. Hutchinson, Limb kinematics, kinetics and muscle dynamics during the sit-to-stand transition in greyhounds. *Front. Bioeng. Biotechnol.* **6**, 162 (2018).
93. S. M. Gatesy, A. R. Manafzadeh, P. J. Bishop, M. L. Turner, R. E. Kambic, A. R. Cuff, J. R. Hutchinson, A proposed standard for quantifying 3-D hindlimb poses in living and extinct archosaurs. *J. Anat.* **241**, 101–118 (2022).
94. A. R. Manafzadeh, S. M. Gatesy, Paleobiological reconstructions of articular function require all six degrees of freedom. *J. Anat.* **239**, 1516–1524 (2021).
95. V. Allen, R. M. Elsey, N. Jones, J. Wright, J. R. Hutchinson, Functional specialization and ontogenetic scaling of limb anatomy in *Alligator mississippiensis*. *J. Anat.* **216**, 423–445 (2010).
96. A. R. Cuff, A. L. A. Wiseman, P. J. Bishop, K. B. Michel, R. Gaignet, J. R. Hutchinson, Anatomically grounded estimation of hindlimb muscle sizes in Archosauria. *J. Anat.* **242**, 289–311 (2023).
97. M. A. Wright, K. E. Sears, S. E. Pierce, Comparison of hindlimb muscle architecture properties in small-bodied, generalist mammals suggests similarity in soft tissue anatomy. *J. Mamm. Evol.* **29**, 477–491 (2022).
98. N. E. Campione, D. C. Evans, A universal scaling relationship between body mass and proximal limb bone dimensions in quadrupedal terrestrial animals. *BMC Biol.* **10**, 60 (2012).
99. J. A. E. Andersson, J. Gillis, G. Horn, J. B. Rawlings, M. Diehl, CasADi: A software framework for nonlinear optimization and optimal control. *Math. Program. Comput.* **11**, 1–36 (2019).
100. M. A. Sherman, A. Seth, S. L. Delp, in *ASME 2013 International Design Engineering Technical Conference* (American Society of Mechanical Engineers, 2013), pp. 1–9.
101. N. E. Bunderson, J. L. McKay, L. H. Ting, T. J. Burkholder, Directional constraint of endpoint force emerges from hindlimb anatomy. *J. Exp. Biol.* **213**, 2131–2141 (2010).
102. J. M. Inouye, J. J. Kutch, F. J. Valero-Cuevas, in *The Human Hand as an Inspiration for Robot Hand Development,* R. Balasubramanian, V. J. Santos, Eds. (Springer Cham, 2014), pp. 247–266.
103. E. Paradis, J. Claude, K. Strimmer, APE: Analysis of phylogenetics and evolution in R language. *Bioinformatics* **20**, 289–290 (2004).
104. L. J. Revell, phytools: An R package for phylogenetic comparative biology (and other things). *Methods Ecol. Evol.* **3**, 217–223 (2012).
105. R Core Team, *R: A Language and Environment for Statistical Computing* (R Foundation for Statistical Computing, 2021).
106. J. Alroy, C. Marshall, A. Miller, The Paleobiology Database (2012); https://paleobiodb.org/.
107. W. N. Venables, B. D. Ripley, *Modern Applied Statistics with S* (Springer, ed. 4, 2002).
108. P. Fahn-Lai, A. A. Biewener, S. E. Pierce, Broad similarities in shoulder muscle architecture and organization across two amniotes: Implications for reconstructing non-mammalian synapsids. *PeerJ* **8**, e8556 (2020).
109. V. Allen, R. E. Kambic, S. M. Gatesy, J. R. Hutchinson, Gearing effects of the patella (knee extensor muscle sesamoid) of the helmeted guineafowl during terrestrial locomotion. *J. Zool.* **303**, 178–187 (2017).
110. P. J. Bishop, K. B. Michel, A. Falisse, A. R. Cuff, V. R. Allen, F. De Groote, J. R. Hutchinson, Computational modelling of muscle fibre operating ranges in the hindlimb of a small ground bird (*Eudromia elegans*), with implications for modelling locomotion in extinct species. *PLOS Comput. Biol.* **17**, 1008843 (2021).
111. S. C. Rewcastle, Form and function in lacertilian knee and mesotarsal joints; a contribution to the analysis of sprawling locomotion. *J. Zool.* **191**, 147–170 (1980).
112. A. S. Romer, Crocodilian Pelvic Musculature and Their Avian and Reptilian Homologues. Bull. Am. Mus. Nat. Hist. 48, 533–552 (1923).
113. L. Cong, L.-H. Hou, X.-C. Wu, *The Gross Anatomy of Alligator sinensis Fauvel* (Beijing Science Press, 1998).
114. M. T. Carrano, J. R. Hutchinson, Pelvic and hindlimb musculature of *Tyrannosaurus rex* (Dinosauria: Theropoda). *J. Morphol.* **253**, 207–228 (2002).
115. D. Brinkman, The hind limb step cycle of *Caiman sclerops* and the mechanics of the crocodile tarsus and metatarsus. *Can. J. Zool.* **58**, 2187–2200 (1980).
116. D. C. Suzuki, K. Y. Tanaka, S. Hayashi, Myology of crocodiles III: Pelvic girdle and hindlimb. *Fossils* **90**, 37–60 (2011).
117. A. Otero, P. A. Gallina, Y. Herrera, Pelvic musculature and function of *Caiman latirostris*. *Herpetol. J.* **20**, 173–184 (2010).
118. M. L. Turner, S. M. Gatesy, Alligators employ intermetatarsal reconfiguration to modulate plantigrade ground contact. *J. Exp. Biol.* **224**, jeb242240 (2021).
119. M. L. Turner, S. M. Gatesy, Inner workings of the alligator ankle reveal the mechanistic origins of archosaur locomotor diversity. *J. Anat.* **242**, 592–606 (2023).
120. S. Regnault, P. Fahn-Lai, R. M. Norris, S. E. Pierce, Shoulder muscle architecture in the echidna (Monotremata: *Tachyglossus aculeatus*) indicates conserved functional properties. *J. Mamm. Evol.* **27**, 591–603 (2020).
121. P. P. Gambaryan, A. A. Aristov, J. M. Dixon, G. Y. Zubtsova, Peculiarities of the hind limb musculature in monotremes: An anatomical description and functional approach . *Russ. J. Theriol.* **1**, 1–36 (2002).
122. C. Westling, *Anatomische Untersuchungen über Echidna*. *Bihang till Kongl Svenska Vetenskaps-Akademiens handlingar* (P.A. Norstedt & söner, 1889).
123. F. A. Jenkins Jr., D. McClearn, Mechanisms of hind foot reversal in climbing mammals. *J. Morphol.* **182**, 197–219 (1984).
124. R. N. Felice, K. D. Angielczyk, in *Early Evolutionary History of the Synapsida,* C. F. Kammerer, K. D. Angielczyk, J. Fröbisch, Eds. (Springer, 2014), pp. 25–51.
125. D. M. S. Watson, The anomodont skeleton. *Trans. Zool. Soc. Lond.* **29**, 131–209 (1960).
126. R. Broom, On the pelvis and sacrum of dicynodon. *Rec. Albany Mus.* **3**, 327–330 (1925).
127. H. S. Pearson, A dicynodont reptile reconstructed. *J. Zool.* **94**, 827–855 (1924).
128. R. Govender, P. J. Hancox, A. M. Yates, Re-evaluation of the postcranial skeleton of the Triassic dicynodont *Kannemeyeria simocephalus* from the *Cynognathus* Assemblage Zone (Subzone B) of South Africa. *Palaeontol. afr.* **43**, 19–37 (2008).

129. R. Govender, Description of the postcranial anatomy of *Aulacephalodon baini* and its possible relationship with '*Aulacephalodon peavoti*'. *S. Afr. J. Sci.* **104**, 479–486 (2008).
130. G. M. King, The postcranial skeleton of *Kingoria nowacki* (von Huene) (Therapsida: Dicynodontia). *Zool. J. Linn. Soc.* **84**, 263–289 (1985).
131. E. H. Colbert, The Mammal-like reptile *Lycaenops*. Bull. Am. Mus. Nat. Hist. 89, 353–404 (1948).
132. R. Broom, On the structure of the mammal-like reptiles of the sub-order gorgonopsia. *Phil. Trans. R. Soc. Lond. B* **218**, 345–371 (1930).
133. C. A. Sidor, New information on gorgonopsian pedal morphology based on articulated material from Zambia. *J. Afr. Earth Sci.* **191**, 104533 (2022).
134. B. Schaeffer, The Morphological and Functional Evolution of the Tarsus in Amphibians and Reptiles Bull. Ame. Mus. Nat. Hist. 78, 395–472 (1941).
135. E.-M. Bendel, C. F. Kammerer, R. M. H. Smith, J. Fröbisch, The postcranial anatomy of *Gorgonops torvus* (Synapsida, Gorgonopsia) from the late Permian of South Africa. *PeerJ* **11**, e15378 (2023).
136. T. S. Kemp, The skeleton of a baurioid therocephalian therapsid from the Lower Triassic (*Lystrosaurus* Zone) of South Africa. *J. Vertebr. Paleontol.* **6**, 215–232 (1986).
137. A. K. Huttenlocker, J. Botha, C. Browning, Z. Kulik, M. Tshibalanganda, A. du Plessis, A Gulliver *Scaloposaurus* (Therapsida, Therocephalia) from the Katberg Formation of South Africa and its implication for Lilliput assemblages during the Early Triassic recovery. *J. Afr. Earth Sci.* **196**, 104720 (2022).
138. S. H. Haughton, On some new therapsid genera. *Ann. S. Afr. Mus.* **28**, 55–78 (1929).
139. B. Schaeffer, The pes of *Bauria cynops* Broom. *American Museum Novitates* (American Museum of Natural History, 1941).
140. F. Abdala, N. P. Giannini, Gomphodont cynodonts of the Chañares Formation: The analysis of an ontogenetic sequence. *J. Vertebr. Paleontol.* **20**, 501–506 (2000).
141. F. S. Filippini, F. Abdala, G. H. Cassini, Body mass estimation in Triassic cynodonts from Argentina based on limb variables. *Acta Palaeontol. Pol.* **67**, 543–557 (2022).
142. J. Liu, V. P. Schneider, P. E. Olsen, The postcranial skeleton of *Boreogomphodon* (Cynodontia: Traversodontidae) from the Upper Triassic of North Carolina, USA and the comparison with other traversodontids. *PeerJ* **5**, e3521 (2017).
143. J. Benoit, M. Nxumalo, L. A. Norton, V. Fernandez, L. C. Gaetano, B. Rubidge, F. Abdala, Synchrotron scanning sheds new light on *Lumkuia fuzzi* (Therapsida, Cynodontia) from the Middle Triassic of South Africa and its phylogenetic placement. *J. Afr. Earth Sci.* **196**, 104689 (2022).
144. A. S. Romer, A. D. Lewis, The Chañares (Argentina) Triassic reptile fauna. XIX. Postcranial materials of the cynodonts *Probelesodon* and *Probainognathus*. *Breviora* **407**, 1–27 (1973).
145. T. V. De Oliveira, M. B. Soares, C. L. Schultz, *Trucidocynodon riograndensis* gen. nov. *et* sp. nov. (Eucynodontia), a new cynodont from the Brazilian Upper Triassic (Santa Maria Formation). *Zootaxa* **2382**, 1–71 (2010).
146. M. L. Guignard, A. G. Martinelli, M. B. Soares, The postcranial anatomy of *Brasilodon quadrangularis* and the acquisition of mammaliaform traits among non-mammaliaform cynodonts. *PLOS ONE* **14**, e0216672 (2019).
147. V. Fernandez, F. Abdala, K. J. Carlson, D. C. Cook, B. S. Rubidge, A. Yates, P. Tafforeau, Synchrotron reveals Early Triassic odd couple: Injured amphibian and aestivating therapsid share burrow. *PLOS ONE* **8**, e64978 (2013).
148. J. F. Bonaparte, Descripción del esqueleto postcraneano de Exaeretodon (Cynodontia – Traversodontidae). *Acta Geológica Lilloana* **4**, 5–52 (1963).
149. Q. Ji, Z. Luo, S.-a. Ji, A Chinese triconodont mammal and mosaic evolution of the mammalian skeleton. *Nature* **398**, 326–330 (1999).
150. Z.-X. Luo, Q. Ji, New study on dental and skeletal features of the Cretaceous "symmetrodontan" mammal *Zhangheotherium*. *J. Mamm. Evol.* **12**, 337–357 (2005).
151. M. Chen, Z.-X. Luo, Postcranial skeleton of the Cretaceous mammal *Akidolestes cifellii* and its locomotor adaptations. *J. Mamm. Evol.* **20**, 159–189 (2013).
152. B. Krebs, Das Skelett von *Henkelotherium guimarotae* gen. et sp. nov. (Eupantotheria, Mammalia) aus dem Oberen Jura von Portugal. *Berl. Geowiss. Abh.* **A133**, 1–121 (1991).
153. E. S. Grood, W. J. Suntay, A joint coordinate system for the clinical description of three-dimensional motions: Application to the knee. *J. Biomech. Eng.* **105**, 136–144 (1983).
154. S. Ray, Functional and evolutionary aspects of the postcranial anatomy of dicynodonts (Synapsida, Therapsida). *Palaeontology* **49**, 1263–1286 (2006).
155. G. M. King, The postcranial skeleton of *Robertia broomiana*, an early dicynodont (Reptilia, Therapsida) from the South African Karoo. *Ann. S. Afr. Mus* **84**, 203–231 (1981).
156. P. A. Pravoslavev, *Gorgonopsidae from the North Dwina Excavations of V.P. Amalitzki* (U.S.S.R. Academy of Sciences, 1927).
157. F. Broili, J. Schröder, Über die Skelettrests einers Gorgonopsiers aus den unteren Beaufort-Schichten. *Sitzungsberichte der mathematisch-naturwissenchaftlichen Abteilung der Baierischen Akademie der Wissenschaften zu München*, 279–330 (1935).
158. F. von Huene, Die Theriodontier des ostafrikanischen Ruhuhu-Gebietes in der Tübinger Sammlung. *Neues Jahrb. Geol. Paläontol.* **92**, 47 (1950).
159. L. D. Boonstra, The Gorgonopsians, *Aelurognathus microdon* and *Hipposaurus boonstrai*, reconstructed. *Ann. S. Afr. Mus.* **42**, 29–31 (1955).
160. D. M. S. Watson, On the skeleton of a bauriamorph reptile. *Proc. Zool. Soc. Lond.* **101**, 1163–1205 (1931).
161. A. S. Brink, On the skeleton of *Aneugomphius ictidoceps* Broom and Robinson. *Palaeontol. afr.* **5**, 29–37 (1958).
162. W. K. Gregory, C. L. Camp, Studies in Comparative Myology and Osteology. Bull. Am. Mus. Nat. Hist. 38, 447–563 (1918).
163. A. S. Brink, A study of the skeleton of *Diademodon*. *Palaeontol. afr.* **3**, 3–46 (1955).
164. Z. Kielan-Jaworowska, P. P. Gambaryan, Postcranial anatomy and habits of Asian multituberculate mammals. *Fossils Strata* **36**, 1–92 (1994).
165. C.-F. Zhou, S. Wu, T. Martin, Z.-X. Luo, A Jurassic mammaliaform and the earliest mammalian evolutionary adaptations. *Nature* **500**, 163–167 (2013).
166. G. T. Yamaguchi, *Dynamic Modeling of Musculoskeletal Motion: A Vectorized Approach for Biomechanical Analysis in Three Dimensions*. (Springer, 2001).
167. W. M. Murray, S. L. Delp, T. S. Buchanan, Variation of muscle moment arms with elbow and forearm position. *J. Biomech.* **28**, 513–525 (1995).
168. H. L. Richards, P. J. Bishop, D. P. Hocking, J. W. Adams, A. R. Evans, Low elbow mobility indicates unique forelimb posture and function in a giant extinct marsupial. *J. Anat.* **238**, 1425–1441 (2021).
169. W. H. Simon, Scale effects in animal joints. I. Articular cartilage thickness and compressive stress. *Arthritis Rheum.* **13**, 244–255 (1970).
170. J. Malda, J. C. de Grauw, K. E. M. Benders, M. J. L. Kik, C. H. A. van de Lest, L. B. Creemers, W. J. A. Dhert, P. R. van Weeren, Of mice, men and elephants: The relation between articular cartilage thickness and body mass. *PLOS ONE* **8**, e57683 (2013).
171. C. M. Holliday, R. C. Ridgely, J. C. Sedlmayr, L. M. Witmer, Cartilaginous epiphyses in extant archosaurs and their implications for reconstructing limb function in dinosaurs. *PLOS ONE* **5**, e13120 (2010).
172. F. J. Valero-Cuevas, F. E. Zajac, C. G. Burgar, Large index-fingertip forces are produced by subject-independent patterns of muscle excitation. *J. Biomech.* **31**, 693–703 (1998).
173. F. J. Valero-Cuevas, B. A. Cohn, H. F. Yngvason, E. L. Lawrence, Exploring the high-dimensional structure of muscle redundancy via subject-specific and generic musculoskeletal models. *J. Biomech.* **48**, 2887–2896 (2015).
174. W. J. Kargo, L. C. Rome, Functional morphology of proximal hindlimb muscles in the frog *Rana pipiens*. *J. Exp. Biol.* **205**, 1987–2004 (2002).
175. J. L. McKay, T. J. Burkholder, L. H. Ting, Biomechanical capabilities influence postural control strategies in the cat hindlimb. *J. Biomech.* **40**, 2254–2260 (2007).
176. W. L. Johnson, D. L. Jindrich, H. Zhong, R. R. Roy, V. R. Edgerton, Application of a rat hindlimb model: A prediction of force spaces reachable through stimulation of nerve fascicles. *IEEE Trans. Biomed. Eng.* **58**, 3328–3338 (2011).
177. E. A. Eberhard, "Modelling the mechanics of jumping in frogs using new computational and robotic methods," thesis, Royal Veterinary College (2019).
178. A. Wächter, L. T. Biegler, On the implementation of an interior-point filter line-search algorithm for large-scale nonlinear programming. *Math. Program.* **106**, 25–57 (2006).
179. R. J. van Arkel, L. Modenese, A. T. M. Phillips, J. R. T. Jeffers, Hip abduction can prevent posterior edge loading of hip replacements. *J. Orthop. Res.* **31**, 1172–1179 (2013).
180. L. Modenese, A. Gopalakrishnan, A. T. M. Phillips, Application of a falsification strategy to a musculoskeletal model of the lower limb and accuracy of the predicted hip contact force vector. *J. Biomech.* **46**, 1193–1200 (2013).
181. D. B. Baier, S. M. Gatesy, F. A. Jenkins Jr., A critical ligamentous mechanism in the evolution of avian flight. *Nature* **445**, 307–310 (2007).
182. S. B. Lippitt, J. E. Vanderhooft, S. L. Harris, J. A. Sidles, D. T. Harryman II, F. A. Matsen III, Glenohumeral stability from concavity-compression: A quantitative analysis. *J. Shoulder Elbow Surg.* **2**, 27–35 (1993).
183. S. Regnault, P. Fahn-Lai, S. E. Pierce, Validation of an echidna forelimb musculoskeletal model using XROMM and diceCT. *Front. Bioeng. Biotechnol.* **9**, 751518 (2021).
184. L. M. Witmer, in *Functional Morphology in Vertebrate Paleontology,* J. J. Thomason, Ed. (Cambridge Univ. Press, 1995), pp. 19–33.
185. L. D. Boonstra, The girdles and Limbs of the pristerognathid Therocephalia. *Ann. S. Afr. Mus.* **48**, 121–161 (1964).
186. L. C. Pusch, C. F. Kammerer, J. Fröbisch, The origin and evolution of Cynodontia (Synapsida, Therapsida): Reassessment of the phylogeny and systematics of the earliest members of this clade using 3D-imaging technologies. *Anat. Rec.* **307**, 1634–1730 (2024).
187. J. J. Kutch, F. J. Valero-Cuevas, Muscle redundancy does not imply robustness to muscle dysfunction. *J. Biomech.* **44**, 1264–1270 (2011).
188. B. A. Cohn, M. Szedlák, B. Gärtner, F. J. Valero-Cuevas, Feasibility theory reconciles and informs alternative approaches to neuromuscular control. *Front. Comput. Neurosci.* **12**, 62 (2018).
189. F. R. Parrington, The evolution of the mammalian femur. *J. Zool.* **137**, 285–298 (1961).
190. M. A. Ashley-Ross, The comparative myology of the thigh and crus in the salamanders *Ambystoma tigrinum* and *Dicamptodon tenebrosus*. *J. Morphol.* **211**, 147–163 (1992).
191. J. C. Walthall, M. A. Ashley-Ross, Postcranial myology of the California Newt, *Taricha torosa*. *Anat. Rec. A Discov. Mol. Cell. Evol. Biol* **288**, 46–57 (2006).

Acknowledgments: Special thanks are due to the museum curatorial and collections staff for access to specimens in care: K. Angielczyk, E. Biedron, J. Botha, C. Browning, E. Butler, C. Byrd, M. Day, J. Escobar, M. Ezcurra, A. Gishlick, R. González, C. Green, S. Jirah, S. Johnston, A. Kowalczyk, A. Krahl, M. Lowe, A. Martinelli, R. Masters, C. Mehling, A. Millhouse, M. Omura, P. Ortiz, O. Rauhut, B. Rubidge, C. Sidor, W. Simpson, Z. Skosan, R. Stebbings, A. Stroup, H. Sues, I. Werneburg, and B. Zipfel. Digitization of fossil material was made possible by M. Day, V. Fernandez, S. Johnston, S. Regnault, and M. Wright, and their assistance is much appreciated. We thank M. Wright, R. Brocklehurst, A. Biewener, C. Richards, E. Eberhard, A. Manafzadeh, S. Gatesy, E. Herbst, D. Polet, F. DeGroote, and J. Cannon for discussion and feedback, and two reviewers for constructive comments on prior manuscript drafts. **Funding:** This work was supported by the US National Science Foundation (grants DEB-1754459 and EAR-2122115 to S.E.P.) and the William F. Milton Fund, Harvard University (to S.E.P.), and published by a grant from the Wetmore Colles Fund, Harvard University (to P.J.B.). **Author contributions:** Both authors contributed to conceptualization, methodology, resources, investigation, data curation, formal analysis, software, visualization, funding acquisition, and manuscript writing. **Competing interests:** The authors declare that they have no competing interests. **Data and materials availability:** All data needed to evaluate the conclusions in the paper are present in the paper and/or the Supplementary Materials. The complete set of the Supplementary Materials files (data S1 to S4) is available through Harvard University's Dataverse Repository at https://doi.org/10.7910/DVN/3EI9SY. Underlying fossil scan data are accessioned with the institutions that house the original fossil specimens or are available via MorphoSource; see data S1 for full details on each specimen's data.

Submitted 24 June 2024
Accepted 20 September 2024
Published 25 October 2024
10.1126/sciadv.adr2722